CHARACTERIZATION OF ADHESIVES AT ROOM AND ELEVATED TEMPERATURES

A Thesis by

Santhosh Kumar Nedukanjirathingal

M. Tech, Regional Engineering College, Warangal, India, 2002

B. Tech, Cochin University of Science & Technology, Cochin, India, 1999

Submitted to the Department of Aerospace Engineering
and the faculty of the Graduate School of
Wichita State University
in partial fulfillment of
the requirements for the degree of
Master of Science

July 2006

CHARACTERIZATION OF ADHESIVES AT ROOM AND ELEVATED TEMPERATURES

I have examined the final copy of this thesis for form and content, and recommend that it be accepted in partial fulfillment of the requirements for the degree of Master of Science, with a major in Aerospace Engineering.

_____
Charles Yang, Committee Chair

We have read this thesis and recommend its acceptance:

_____
Bert Smith, Committee Member

_____
Hamid M. Lankarani, Committee Member

DEDICATION

To my parents, sister, relatives, and friends

ACKNOWLEDGEMENTS

A journey is easier when we travel together. Interdependence is certainly more valuable than independence. This thesis is the result of two years of work whereby I have been accompanied and supported by many people. It is a pleasant aspect that I have now the opportunity to express my gratitude to all of them.

I wish to express my sincere gratitude to my advisor Dr. Charles Yang (Associate Professor, Department of Aerospace Engineering, Wichita State University), for all his help and effort provided during the course of this study at Wichita State University. I am also indebted to the support from NASA Langley Research Center.

My special thanks to Dr. Bert Smith (Professor, Department of Aerospace Engineering, Wichita State University) and Dr. Hamid M. Lankarani (Professor, Department of Mechanical Engineering, Wichita State University) for being my thesis committee members and the advice they have given throughout the course of this study. I am also grateful to Waruna Seneviratne, Research Associate, National Institute for Aviation Research (NIAR), Wichita State University. His support included invaluable accessibility to research facilities at NIAR.

I extend my thanks to Wenjun Sun, Yoon Khian Yap, Govind Ramakrishna Pillai, Ananthram Kota Sashidhar, and Shih Pin Chou who helped me throughout this project in providing support and suggestions.

ABSTRACT

Recent interest in advanced materials has paved the way for exploring joining options besides the traditional mechanical or thermal methods such as riveting or welding. Because of the availability of highly advanced materials, mass production rates and demands for more aesthetic products, adhesive bonding is being used in more applications. Today, interstate signs, semi-trailer panels, aircraft structures, and many other commonly used products are adhesively bonded. Some of the common misconceptions about adhesives are that they are inherently weak, require high operator skill, and are too expensive for production. However, these assumptions are true only when the adhesive joint design is faulty and/or the bonding process is performed incorrectly.

This report includes testing, using single lap joints, of some adhesives both at room and elevated temperatures. Experimental setups for performing the tests are discussed. The shear strengths of various adhesives are determined with titanium adherends. A methodology was developed to determine the approximate value of shear modulus of the adhesive using finite element modeling (FEM) from the ASTM D 3165 test. This was completed in conjunction with experiments using a laser extensometer. Later in the report, correction factors that are used with the laser extensometer data to determine the shear moduli are determined.

TABLE OF CONTENTS

TABLE OF CONTENTS (continued)

LIST OF TABLES

LIST OF FIGURES

LIST OF FIGURES (continued)

LIST OF FIGURES (continued)

Figure Page

LIST OF FIGURES (continued)

Figure Page

CHAPTER 1

INTRODUCTION

This introduction includes topics that are more significant to this thesis and research performed for this thesis. Many researchers came up with the definition of adhesion and adhesives, but a clear definition given by R.C. Patrick [1] was, "adhesion is the phenomenon of causing two materials to be held together, while an adhesive is the material utilized in carrying out this phenomenon." Most of the major developments in this field were in the second half of last century (1950-2000).

Due to many researches conducted in this respective field during the second half of last century, the relevance and applications of this branch of study became very clear and distinct. It found its application in many major fields of engineering and maintenance, say, military, aerospace, microelectronics etc. One of the main reasons that it found in the application of aerospace is because, adhesive joints can reduce the extra weight brought by fastener joints and rivets. Significant weight savings can be implemented using adhesive joints. Therefore the importance of aromatic polyamides and related polymers increased to a great extent. These adhesives possess properties including, excellent thermal stability, solvent resistance, good mechanical properties, radiation resistance, low thermal expansion, wear resistance etc. A good adhesion occurs when the surfaces are held together by interfacial forces and when there is real close contact of surfaces.

Prior to its use, much importance are given to analysis, design and testing of the bonded structures using adhesives. Hence, during adhesive development, standardized tests, using respective test methods and preparation, need to be conducted. This will

provide data and results to compare and evaluate the various adhesion parameters. One of the most important parameters are (1) strength, (2) fracture toughness, and (3) solvent resistance of the bonded joints and the most widely used tests are (1) lap-shear tests for strength comparisons, (2) the "double cantilever beam test" for the fracture toughness of the adhesive joints, and (3)the wedge test to determine the solvent resistance. In this thesis work, the lap-shear test, which is the primary adhesion test method, is discussed and performed for certain adhesives at high temperature and room temperature.

One of the most critical and often overlooked factors that contribute to the success of an adhesive bond is choosing the proper adhesive. The selection process can be divided into four steps;

1. Specify the service requirements of the product or joint, such as load capacity, temperature or expected life.
2. Identify the substrates being joined. Some adhesives bond better to certain materials than to others, and matching the substrate with the right adhesive is important in producing optimal adhesion properties.
3. Determine the manufacturing processes, such as the method used to apply the adhesive to the substrate and the curing conditions.
4. Evaluate these variables, and select the adhesive that best fits the joint's needs.

1.1 Research Focus and Objectives

In most of adhesive-bonded joints load is transferred by shear. Hence, for an efficient design of the joint it will be helpful for a designer if the mechanical properties of the adhesives are already known. The properties includes the shear strength and stiffness

of the adhesives. Kutscha [2] and Kutscha and Hofer [3] clearly stated about the above fact regarding the importance of mechanical properties of adhesives. One of the important conclusion made over years while determining the mechanical properties was the use of thin adhesive film configurations [18]. Some of the widely used tests(ASTM) for determining the mechanical properties are listed as follows [18]:

1. ASTM D1002 – This is a test for determining the strength properties of adhesives in shear. Here, the test specimen is loaded in tension.
2. ASTM D 3165 – This test is for determining the strength properties of adhesives in shear. This is performed by tension loading of single lap-joint laminated assemblies.
3. ASTM D 5656 – This test involves a thick-adherend metal lap-shear joint. It is used for determining the stress-strain behavior of adhesives in shear by tension loading.

The specimen geometries for various tests, ASTM D 1002, ASTM D 3165 and ASTM D 5656 are shown in Figures 1.1, 1.2, and 1.3 respectively.

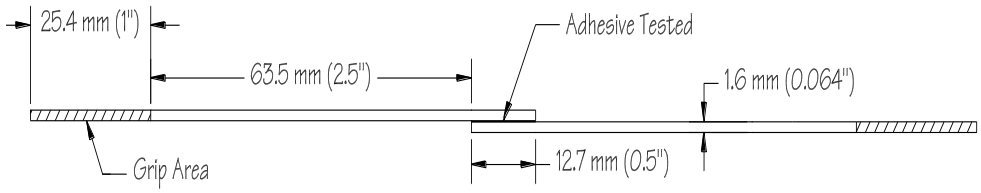

Figure 1.1. Specimen geomtery of ASTM D 1002.

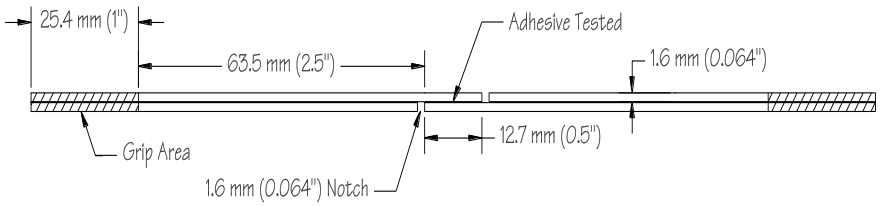

Figure 1.2. Specimen geometry of ASTM D 3165.

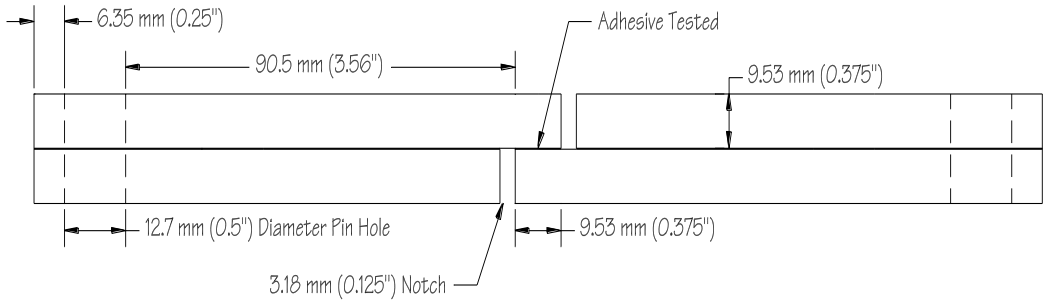

Figure 1.3. Specimen geometry of ASTM D 5656.

This thesis concentrates on studying and analyzing the single lap joint for certain adhesives with titanium as the adherend, at both room and elevated temperatures (600ºF and 750ºF). The objectives are as follows: (1) To determine the failure loads (proportional parameter of shear strength) of various adhesive joints from ASTM D 3165 and ASTM D 1002 tests at both room and elevated temperatures (600ºF and 750ºF), (2) to develop a methodology to determine the shear modulus of adhesives using finite element modeling from ASTM D 3165 tests, and (3) to determine using correction factors, the shear modulus of adhesives from the ASTM D 5656 test while using a laser extensometer with the designed fixture.

The work performed under this task supported the NASA Langley Research Center's (LaRC) investigation of high-temperature adhesives for reduced mass aeroshells. Details of aeroshells are provided in Appendix A. Since reduced mass translates directly into larger payloads, the importance of accomplishing this goal of reducing the mass is common to all planetary missions. Current aeroshell designs typically use metallic structure. Sometimes conventional composite materials are incorporated into the design. The amount of thermal protection required for these materials is relatively great, and resulting aeroshells are relatively massive. There are now new families of high temperature resins and composite material manufacturing techniques that have the potential to significantly reduce mass and improve aeroshell design. The proposed effort is intended to demonstrate that the use of these technologies can result in significant mass reductions (approaching 30 percent) for the primary aeroshell structure and its associated thermal protection system (TPS).

An additional goal was to show that these mass reductions can be obtained at relatively low cost and without the high risk often associated with alternative aeroshell designs or planetary entry systems. The goal was to determine optimized aeroshell system masses for a range of planetary entry environments (including Titan and Neptune) with acceleration loads of 3-20g and peak structural temperatures ranging from 400 to 700^{o}F (for the primary structure that lies behind the TPS). The optimized systems should result in a significant mass savings for relatively less challenging missions (such as Titan aerocapture) and will hopefully go further to enable for more difficult missions (such as Neptune aerocapture). State-of-the-art high-temperature composite materials, resins, and adhesives will then be examined for incorporation into these concepts. The program

verified fabrication methods for lightweight compound curvature aeroshells through the fabrication of representative coupon samples, structural elements, and finally system-level subcomponents, all of which were tested in relevant environments. This effort was a natural extension of work that has already been done to incorporate high-temperature materials into NASA aircraft and reusable launch vehicle (RLV) programs. The effort was built on the heritage of existing aeroshell design, and used a building-block approach that began with the identification and testing of coupon-sized material and adhesive specimens. Once appropriate materials and adhesives were verified for aerocapture in relevant environments, larger-scale system-level components and finally a representative aeroshell prototype were demonstrated. The goal was to advance the technology readiness levels (TRL) of high-temperature structural systems and to maximize their impact on all aspects of aeroshell design.

1.2 Report Organization

This report comprises five chapters. Chapter 1 is the introduction. Chapter 2 contains background information and a literature review on the work completed. The experimental setups, analysis, and procedures used are discussed in Chapter 3. The results of the tests and analyses and discussions are presented in Chapter 4. The conclusion and future work are given in Chapter 5.

CHAPTER 2

LITERATURE REVIEW

Adhesive bonding is capable of being used in load-bearing engineering applications, particularly for joining sheet metals. However, it is also used for a wide range of applications up to large structures used in aerospace applications. Modern structural adhesives are strong but will only work effectively if surface preparation is carried out correctly. Almost all metals can be successfully joined by adhesives. Surface preparations of these metals are, with very limited exceptions, always necessary. For some metals, the requirements for surface preparation are more stringent than others. Different surface preparations are needed for different metals, but all lead to clean the surface.

2.1 Advantages of Adhesive Bonding

The main advantages of adhesive bonding are as follows [4]:

1. Stress: The resulting stress will be more uniformly distributed, and stress concentrations will be lower than with mechanical fastening. In a situation where the loaded surface area cannot be increased, adhesive bonding may be inappropriate.
2. Adherends: One of the main advantages of adhesive bonding is that dissimilar materials can be easily joined, which is not the case with welding, brazing, etc. Also, heat distortion stresses are minimized compared with welding.
3. Surface Area: For a joint, especially a lap joint, stress is distributed over a larger area, which will result in providing a joint with lower stress concentration and improves the strength of the joint.

4. Adhesive joints serve the purpose of a sealant in addition to the fastening.
5. Machine-shop related works and associated costs are minimized.
6. Widely used when the joints are made of softer materials.

2.2 Limitations of Adhesive Bonding

Though it has many advantages as mentioned above, the limitations of adhesive joints are listed below [4, 5]:

1. Adverse effect of chemicals and water on the joint strength.
2. Surface preparation is important for good and reliable joints.
3. Time consumption in preparing the bond is one of the main disadvantages to attain required design strength.
4. Intuitively not considered a stable joint.
5. Temperature limitations, especially in withstanding high temperatures.
6. Many associated components in preparing the joint, like jigs, and fixtures.
7. Safety measures are required when preparing the adhesive bonding.

2.3 Different Types of Adhesives

2.3.1 Natural Adhesives

Natural adhesives are generally set by solvent evaporation. One of the main drawbacks of this type is that, these types have low strength. They are also very susceptible to moisture and mold. The uses of natural adhesives are limited to the joining low-strength and fragile materials. Some of the adhesives that come in this category are animal glues, fish glues, vegetable glues, and casein.

2.3.2 Elastomer Adhesives

These adhesives, elastomer adhesives, are based on natural and synthetic rubbers. These types of adhesives are set by solvent evaporation. The primary disadvantage of such adhesives is relatively low shear strength. The elastomer adhesives suffer from creep, and are hence used for unstressed joints. Whenever the joints include materials such as plastic and rubber, these types of adhesives are very useful. Some fine examples of this category include natural rubbers, polychloroprenes, acrylonitride butadiene, butyl rubber adhesives, etc.

2.3.3 Thermoplastic Adhesives

Usually, most of the thermoplastic adhesives have low/medium shear strength. These types of adhesives may suffer from creep at high loading jut like elastomer adhesives. The excellent resistance to oils is an advantage and very poor resistance to water is a disadvantage of this type of adhesives. Some good examples of this category include polyvinyl alcohol, polyacrylates, silicone resins, polyamides, acrylic acid diesters, polyvinyl acetate etc.

2.3.4 Thermoset Adhesives

Thermoset adhesives have a rigid cross-linked structure. They are polymeric resins which are cured by heat and/or by pressure. Phenolic formaldehyde resins, phenolic neoprene, resorcinol formaldehydes (RF), and epoxy resins falls in to this category.

2.3.5 Toughened Adhesives

"Toughening" was developed in the recent past years. This type of adhesives has rubber-like particles dispersed throughout a glassy solvent. The effect of these particles is to make it resistant to crack propagation, which is one of the main problems faced by the fatigue and fracture groups in an organization, especially manufacturing industry.

2.3.6 High Temperature Adhesives

High temperature adhesives find its application mainly in aerospace industries. A number of adhesives available can operate at higher temperatures than epoxies and phenolics. These adhesives are really expensive and require high cure temperatures; sometimes complicated cure schedules.

2.4 Thermal Properties of Adhesives

At a low enough temperature, a polymer is rigid and glassy, while on heating through the glass transition temperature, it becomes relatively flexible and rubbery. If semicrystalline, the next transition stage will be the melting of the crystallines. At still higher temperatures, polymers decompose chemically.

2.4.1 Glass Transition Temperature

Glass transition temperature (T_g) is the temperature at which a material's characteristics change from that of a glass to that of rubber. For thermoplastics, this glass transition temperature varies widely. At temperatures well below the T_g value, amorphous polymers are hard and stiff. At the same time, at temperatures above T_g , polymers are rubbery. The temperature region in the close proximity of T_g is often called the leathery region. The glass transition is not a sudden transition but a gradual

transition. Polymers are generally rigid and brittle below their glass transition temperature and can undergo plastic deformation above it.

2.5 Surface Preparation and Characterization

One of the few disadvantages of adhesive bonding as a method of fastening is that the surfaces need to be cleaned, and their chemical nature must be coherent in the sense that they must not be powdery or friable. Surface treatment of an adherend prior to adhesive bonding can do one or a combination of the following effects:

- Remove material (oils, greases, weak oxide layers, dust, etc.).
- Modify the surface chemistry.
- Change the surface topography (roughness).

2.6 Surface Preparation of Titanium and Titanium Alloys

One of the main advantages of titanium is its high strength-to-weight ratio. It possesses excellent corrosion resistance, displays high toughness relative to steel and aluminum. The ability of titanium to retain its mechanical properties at very high temperatures makes it applicable in aerospace structural applications, landing gears, blades of gas turbines, nuclear power plants, etc. The main disadvantage of this metal is the cost. The two different crystalline phases of titanium are: (1) the α-phase, a hexagonal, closed-packed form, and (2) the β-phase, a body-centered cubic form. The α-phase is formed when the temperature exceeds 1,500ºF. It is at this phase that it shows a lower strength-to-weight ratio and increased sensitivity to corrosion. The β-phase alloys are stronger, tougher, and resistant to environmental corrosion and at the same time show poor forming characteristics. The metallographic structures of different alloys lead to

different surface structures when etched. Maximum bond strengths with a newly introduced alloy will only be obtained as a result of experiments in which the concentration of reagents and time of treatment are varied over a suitable range. Surface treatment of the titanium-alloy is critical in improving the initial strength and long-term durability of the adhesive joint. These surface treatments help in removing the contaminants on the sample and create a stable adherend surface that is compatible with the adhesive. The primary reason to use titanium adherends is the high temperature involved in planetary missions. Some of the methods of treating the surfaces of bonding are discussed below.

2.6.1 Alkaline Peroxide Etch

1. Vapor degrease and wet-blast with alumina.
2. Immerse for 20 minutes at 140-158ºF in sodium hydroxide, 22.5 ml of hydrogen peroxide, and 1 liter of water at 0.044 lbf.
3. Wash in hot water for at least 10 minutes.
4. Dry in warm air.
5. Preferably, apply a primer coat immediately.

2.6.2 Acid Pre-Etch and Chromic Acid Anodize

1. Degrease.
2. Abrade ideally by grit blasting.
3. Pre-etch at ambient temperature for 10 to 20 minutes in a solution of 4.5 liters of concentrated nitric acid, 0.45 liters of hydrofluoric acid, and 10 liters of water.

4. Place under clean, cold running water, and brush off any black deposits with a clean, stiff-bristle nylon brush.
5. Anodize at 104ºF in 1.5 lbs chromium trioxide and 10 liters of water. Raise the voltage to 20 volts over 5 minutes and hold for 5 to 30 minutes until the metal has developed a distinctive blue color.
6. Spray rinse with cold water.
7. Dry in an air-circulating oven at no greater than 100ºF.

2.6.3 Pasa-Jell

Pasa-Jell products are designed for the treatment of metal surfaces. They are compounds based on a mixture of mineral acids, activators, and inhibitors. Some are inorganically thickened to permit application in localized areas and on vertical or overhead surfaces. The following steps are used in the Pasa-Jell treatment of the titanium adherend surfaces.

1. Degrease with a solvent (methyl ethyl ketone).
2. Grit-blast at 60 psi using 1250μm, 120 high-grade alumina.
3. Apply Pasa-Jell (Pasa-Jell 107 to titanium with brush for 15 minutes.
4. Remove excess with kimwipe tissues soaked with tap water, and check surface acidity with litmus paper.
5. Rinse surface with distilled water, and perform a water break test.
6. Oven dry for 30 minutes at 120ºF.

2.7 Adhesive Joint Design

The advantage of an adhesive joint is that stresses are distributed more uniformly throughout the joint. The concentration of stresses in the small region significantly reduces the load that joints may carry. Hence, the same joint that is adhesively bonded will more uniformly distribute stresses throughout the entire joint, which increases the overall load capacity of the joint by decreasing the load per unit area.

While testing the operating load should be transferred as a shear stress rather than a tensile stress. One of the main disadvantages of adhesive joint is that they are very poor in withstanding peel and cleavage loads. The lap joints and the axial fit joints are the most common joints. Some of the major and common adhesive joints are shown in Figure 2.1. The double lap joint will lower the bending moments and hence will reduce the peel loads.

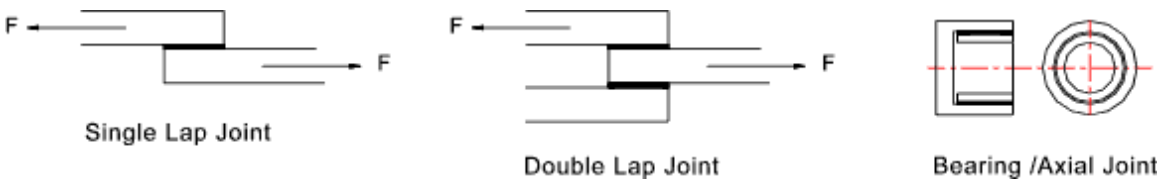

Figure 2.1. Different types of adhesive joints [4].

2.8 Some Aspects of Various Adhesive Tests

Before an adhesive is put into its final use, a detailed analysis regarding design, testing, and reliability of the actual bonded structures is essential. The most widely used tests to characterize these phenomenons are lap shear tests for strength comparisons.

2.8.1 ASTM D 1002

This is one of the most commonly used testing methods (single lap joint) [6] for determining the shear strength properties of adhesives in shear. Here, the specimen is subjected to tension loading. The dimensions of the specimen are shown in the Figure. 2.2.

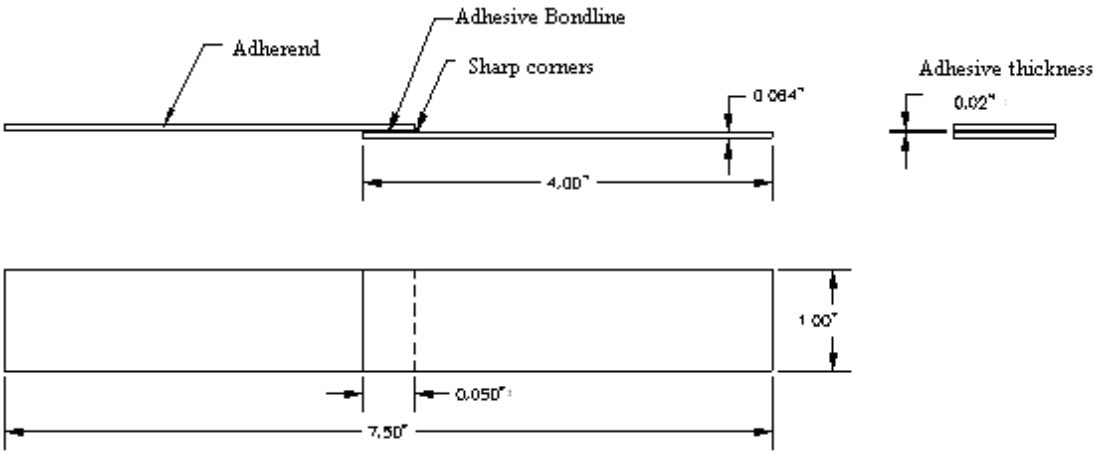

Figure 2.2. Specimen geometry of ASTM D 1002.

Note that this joint is automatically misaligned before it is placed in the testing machine. Some lab-bound tabs at the ends are used to improve the alignment of the specimen. Regardless, the joint will bend during testing, as shown in Figure. 2.3, giving rise to large transverse peel stresses in the adhesive layer. Regardless it is still recommended in ASTM D 1002 and similar standards still recommended that the results are given as average shear stress at failure (i.e., load divided by bond area). The advantages of this single lap test are that it is simple, inexpensive, uses a standard tensile testing machine, etc. Many attempts have been made to improve the single lap test. These include the

ASTM D 3165 standard where some of the bending is prevented compared with the simple, single lap joint. The test gives the apparent average shear strength. It is to be noted that this test is not for designing actual bonded structures or obtaining true shear strength of the adhesive joint. The average shear strength from the test is given by

$$\tau_m = \frac{P}{bL} \tag{2.1}$$

In the above equation, τ_m is the apparent average shear strength, P is the applied load, and b and L are joint width and length, respectively.

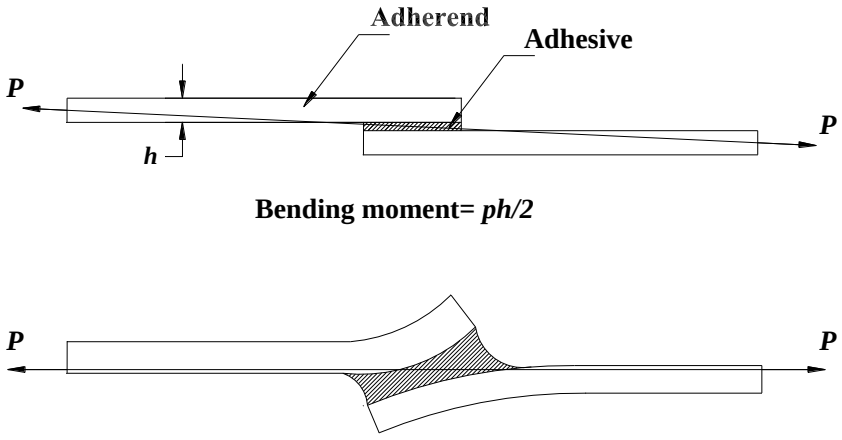

Figure 2.3. Effect of bending moment along adhesive bondline to give peel stress, thereby reducing the joint strength**.**

From various studies it was established that the stress distributions within the sample are affected by (1) adherend modulus and thickness, (2) adhesive moduli and thickness, and (3) bond overlap length. These factors cannot be neglected before testing since they can have very high influence on the bond strengths obtained. To account for the non-uniform shear stress distribution along the bond- line, Volkersen [7] proposed a shear lag model. According to the model adhesive deforms only in shear and the

adherends are deformed only in tension. As per the model, the shear stress distribution along any point "*x*" along the bondline is given by (*x*=0 means the center of the lap joint)

$$\tau(x) = \frac{P\omega}{2\sinh(\frac{\omega l}{2})}\cosh(\omega x) + \frac{P\omega}{2\cosh(\frac{\omega l}{2})}\sinh(\omega x)[\frac{E_2 h_2 - E_1 h_1}{E_2 h_2 + E_1 h_1}] \tag{2.2}$$

where ω is calculated as

$$\omega = \sqrt{\frac{G}{t}(\frac{E_2 h_2 + E_1 h_1}{E_1 h_1 E_2 h_2})} \tag{2.3}$$

In the above equations, *P* is the force, *h* is the adherend thickness, *E* is the Young's modulus of the adherends, *t* is the adhesive thickness, *G* is the shear modulus of adhesive, and *l* is the length of the overlap.

One of the main assumptions in Volkersen's shear lag approach is that the adhesive and the adherend are linearly elastic. According to the model, the adherend tensile stress decreases progressively from the loaded end to the unloaded end along the width of the specimen, shear strain and shear stress in the adhesive are maximum at the ends and minimum at the center. It was found that, dissimilar adherends will lead to an asymmetric shear stress distribution.

One of the main factors Volkersen ignored was the bending moments in the joint due to nonlinear load application, which may result in peeling. Any amount of bending of the adherends alters the direction of the loadline in the test sample, which by itself creates a bending moment. This will result in adhesive deformation which will no longer is proportional to the applied load. Goland and Reissner [8] took this bending, into account and introduced a bending moment factor *k*, as

$$M_0 = \frac{kPh}{2} \tag{2.4}$$

where h is the adherend thickness, M_0.is the bending moment and P is the applied load. Goland and Reissner came up with a more non-uniform shear stress profile in the bondline than that by Volkersen's shear lag approach model. One important distinction of Goland and Reissner model is that it predicts the excessive adhesive shear strains at the edges due to elastic bending of the adherends and peel stress (σ_y) acting on the adhesive layer (as shown in Figure 2.3). These excessive shear strains may lead to the failure of the adhesive bond. The peel stress is non-uniform and distributed as given in Figure 2.4. The maximum peel stress is at the edges. According to the model proposed by Goland and Reissner, the value of factor k does not go to zero but approaches 0.2 towards the middle of the bondline. The analysis by Hart-smith [9, 10], however, predicts that this value of k will fall to zero at the center of the bondline. This model also predicts negligible peel stress towards the middle of the bond.

The peel forces affect the bond strength values critically in lap-shear joints. Increasing the length of the overlap or the shear modulus of the adhesive increases the non uniformity and non linearity of the shear stress profile. The uniformity of the shear stress distribution can be increased by increasing the modulus of the adherend, thickness of the adherends, and the bondline thickness.

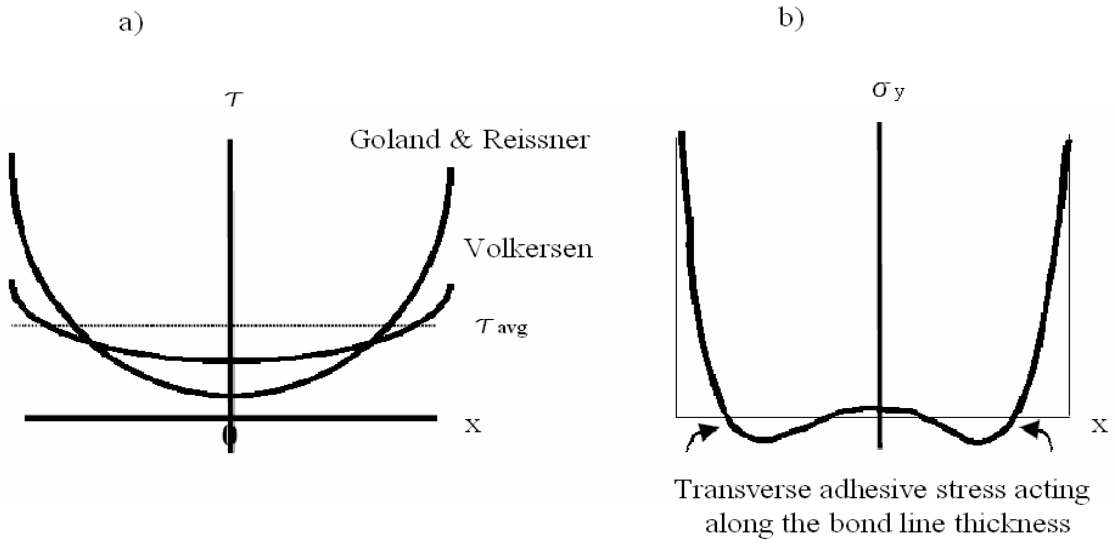

Figure 2.4. (a) Shear strength profiles as given by various analyses; (b) peel stress along the bondline as determined by Goland-Reissner analysis [4].

2.8.2 ASTM D 3165

This test method, ASTM D 3165 [11], given in Figure 2.5, is performed to determine the comparative strengths of adhesives in large area joints when tested on a standard single lap joint specimen. In this ASTM D 3165 test, the joint configuration is similar to the configurations which are commonly found in day-to-day engineering applications. It can be used to develop design parameters for such similar structures and joints. The apparent shear strength of an adhesive thus obtained from the test may differ depending on the type of adherends and bonding process.

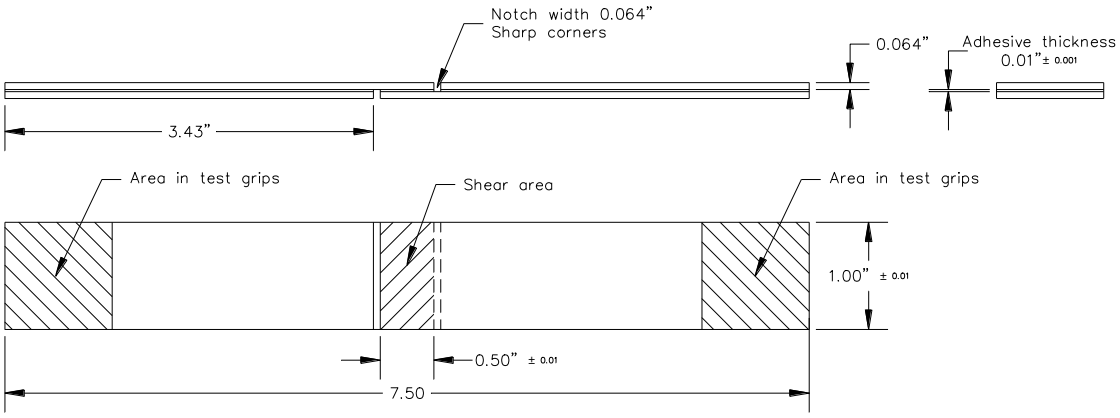

Figure 2.5. Specimen geometry of ASTM D 3165 specimen.

2.8.3 ASTM D 5656, Determination of Stress-Strain Behavior of Adhesives in Shear.

This test method, ASTM D 5656 [12] is used to determine the stress-strain properties of an adhesive in shear by loading the specimen in tension. It also helps to establish the proportional limit of the stress-strain relationship, in a stress-strain curve. The stress-strain data thus determined find its application as a major input in many analytical models, which are primarily used in designing joints.. This test is often called the "The Thick Adherend Shear Test (TAST)." The ASTM D 5656 specimen geometry is shown in Figure 2.6. In effect, it attempts to minimize the effect of differential straining by using stiff and thick metallic adherends. In this form of joint, there is a considerable increase in the flexural and tensile stiffness of the adherends.

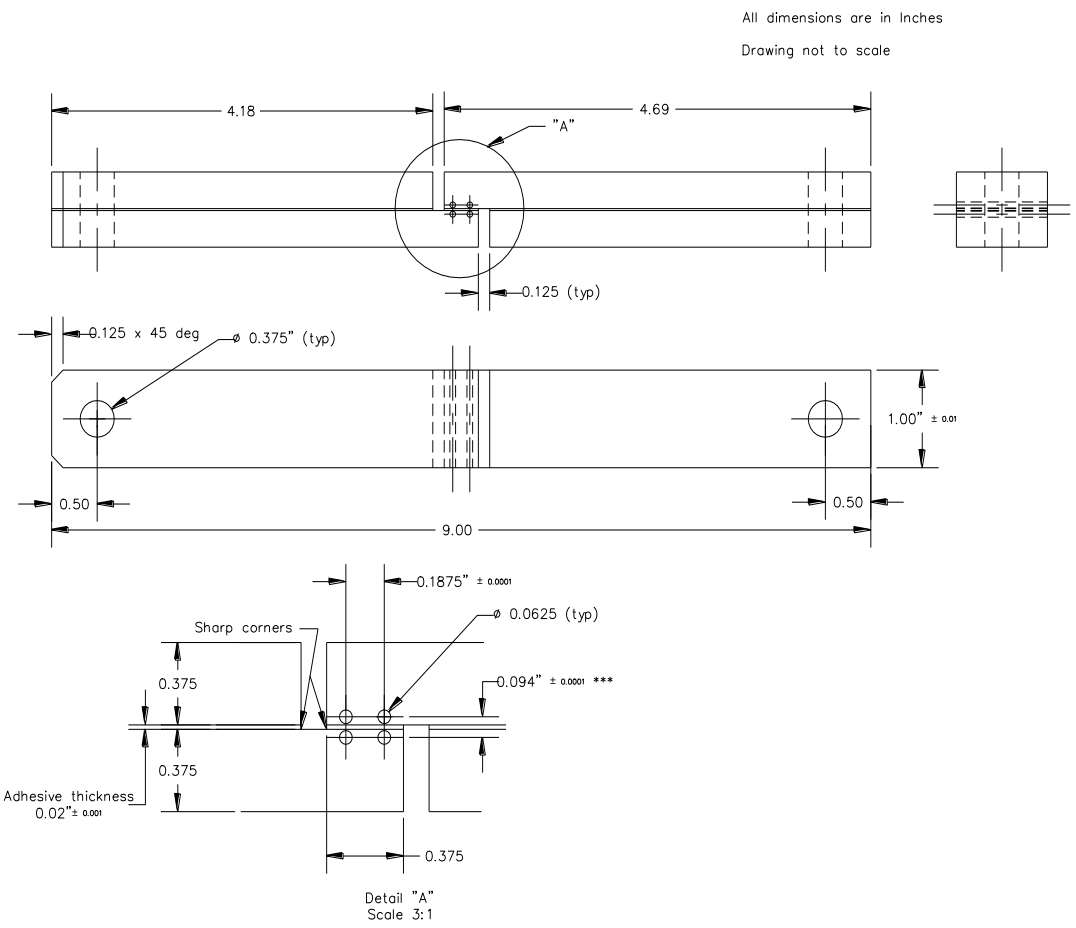

Figure 2.6. Specimen geometry of ASTM D 5656 specimen.

The combination of these two properties (stiff and thick metallic adherends) has led to the popular belief that the adhesive is now in a state of shear and there are no significant transverse peeling loads. It should be noted that, although this test method can be used to generate characteristic shear-strain curves and evaluate adhesive properties, is very complicated and requires careful preparation of the specimen, load introduction, and sensitive measurement instruments (KGR-type extensometer). The KGR-1 device [12] is designed to measure the relative displacement between two points across the adhesive

using a three-pin configuration, as shown in Figure 2.7. The third pin is used to align the device during loading when rotation occurs.

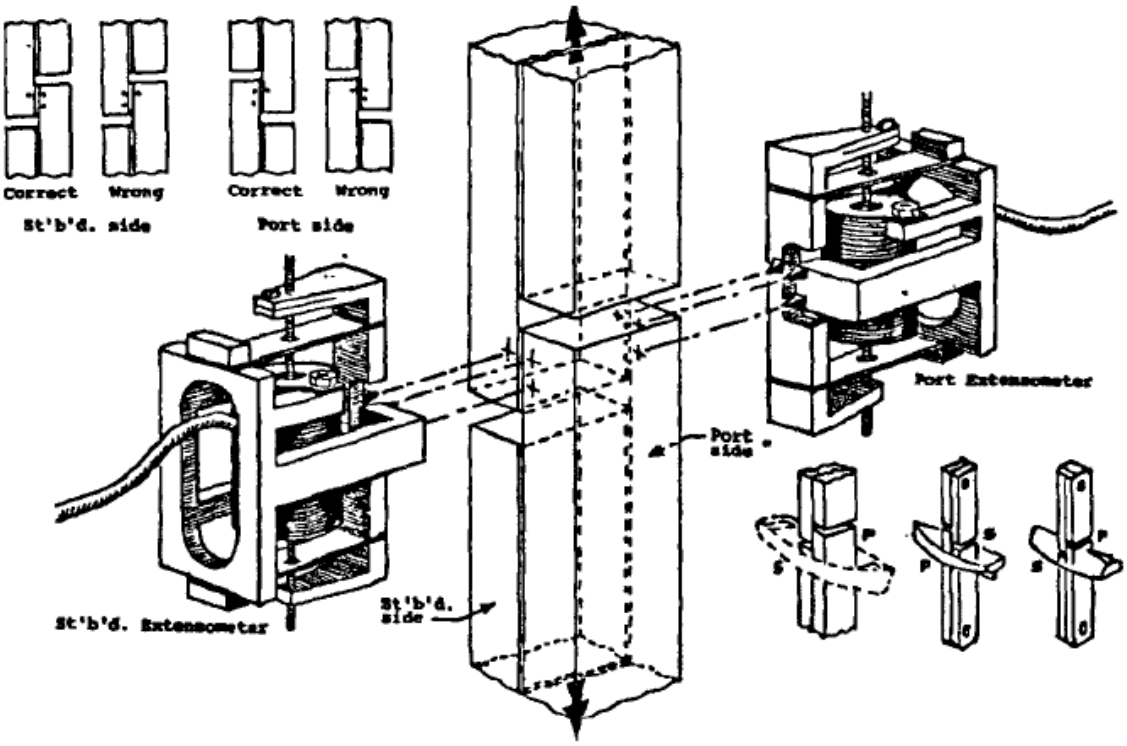

Figure 2.7. Mounting of KGR-1 device on ASTM D 5656 specimen [12].

A small fixture [13], a modified version, was designed and machined at Wichita State University (WSU) to be attached to a mechanical extensometer (MTS) model number 632.11B-20. The WSU device uses the same concept as the KGR-1 device; however, several modifications were made to enable the device to collect more accurate data, which is discussed below. The fixture attached to an extensometer is shown in Figure 2.8.

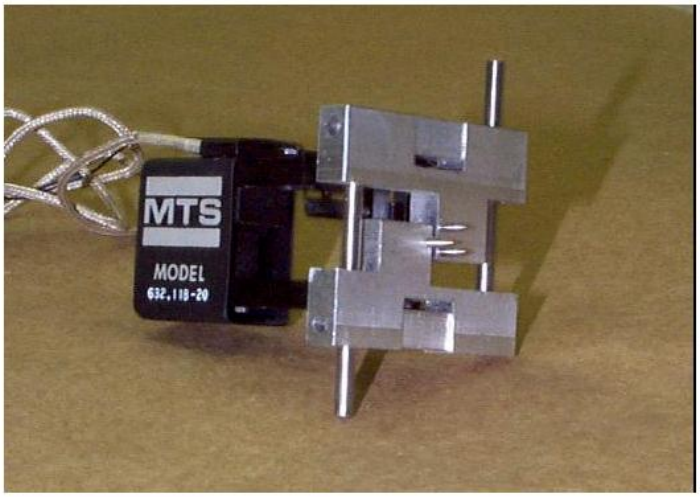

Figure 2.8. Fixture and the device designed at WSU (three-pin configuration) [13].

The KGR-type device was used to gather data for characterizing the stress-strain relationship of adhesives using ASTM D 5656 test specimens. ASTM specifications are designed around the KGR-1 device, which has a three-pin configuration that rests on the surface of the specimen. Initially, the fixture used was made with the same three-pin configuration. While using this, three-pin fixture, the large scatter in the tests was due to the following:

- Slippage of the mounting pins on the surface of the ASTM D 5656 specimen.
- Stretching of the adherend between the holes under the tensile load. While using the KGR-type device, even though the stretching of adherend was not significant, the error due to the slippage of the mounting pins was significantly high [18].
- Rotation of the KGR-type fixture while under load. Even small rotations are significant due to the small displacements being measured.

It was decided that these discrepancies could be reduced in two ways: (1) adding a fourth pin to reduce any unwanted rotation of the device, and (2) drilling small holes into the adherend of the same size as the pins [14, 15]. By drilling mounting holes into the adherend, any slippage of the measuring pins on the surface of the specimen was eliminated. Moreover, the need for any spring force used in mounting the device was eliminated, since the fixture could slide into the pre-drilled holes on the specimen. Hence, another fixture was designed and machined at WSU (a four-pin configuration) to mount the extensometer, as shown in Figure 2.9. The modified four-pin KGR type extensometer [16] used in this investigation was provided with knife edges so that extra calibration was not necessary. Since the specimen extends in the loading direction, the knife edges allowed the extensometer arms to rotate so that the pins remained perpendicular to the specimen.

Figure 2.9. Modified KGR- type extensometer (four-pin configuration) [16].

To determine the shear modulus of the adhesive, the displacements where the extensometer pins are fixed at points A, B, C, and D as shown in Figure 2.10, are

measured. These displacements are used to determine the approximate value of shear strain. The real shear modulus of an adhesive using ASTM standard is calculated by incorporating some correction factors [13].

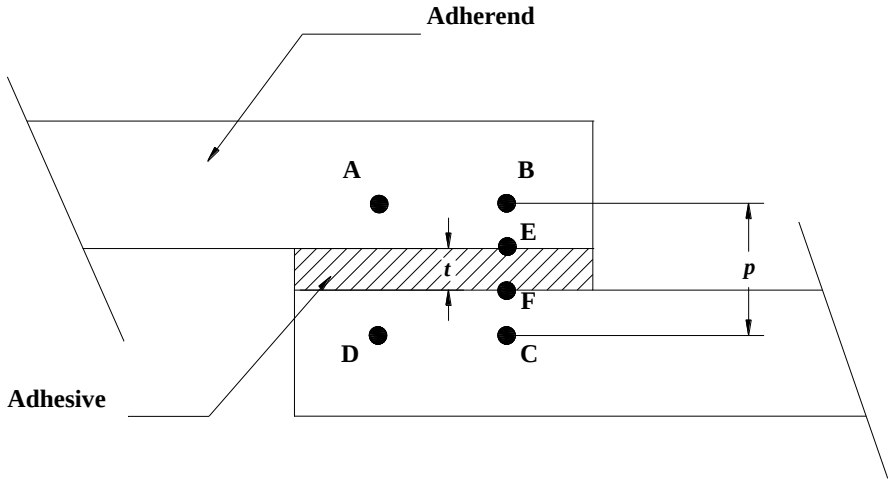

Figure 2.10 Center portion of ASTM D 5656 specimen
(A, B, C, and D are points where holes are drilled).

2.9 Failure Modes of Adhesive Joints

To gain a full understanding of the properties of the adhesives and the joint being investigated, the mode of failure must be characterized. In adhesive technology, there are three typical characterizations for the failure mode of an adhesive joint, as shown in Figure 2.11:

- Cohesive failure, characterized by failure within the adhesive.
- Adhesive failure, characterized by a failure of the joint at the adhesive/adherend interface and typically caused by inadequate surface preparation, chemically and/or mechanically. Specimens that fail adhesively tend to have excessive peel stresses that lead to failure and often do not yield a strength value for the adhesive joint but rather indicate unsuitable surface qualities of the adherends.

- Substrate failure, characterized by failure of the adherends instead of the adhesive. In metals, this occurs when the adherends yield. In composites, the laminate typically fails by the way of interlamina failure, i.e., the matrix between the plies fails. In substrates, failures occur when the adhesive is stronger than the adherend in the joint being tested.

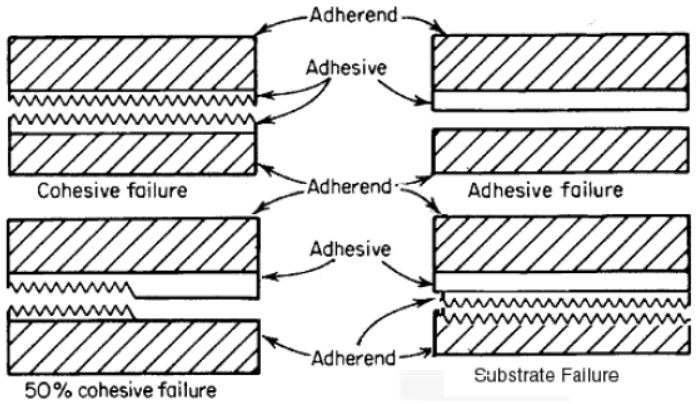

Figure 2.11. Failure modes of the bond line in adhesive joints [17].

CHAPTER 3

EXPERIMENTAL SETUPS AND ANALYSIS

3.1 Test Matrix

The test matrix was developed based on the adhesives to be tested. Specimens were made based on the batches shown in Figure 3.1. They were tested and the data were recorded (failure load, type of failure, etc.). There were different sets of specimens for both ASTM D 3165 and ASTM D 1002, which were to be tested at both room temperature and elevated temperature. The fixture for mounting the specimen was designed to serve the purpose for both temperature tests. The test setups at room temperature were almost the same for ASTM D 3165 and ASTM D 1002.

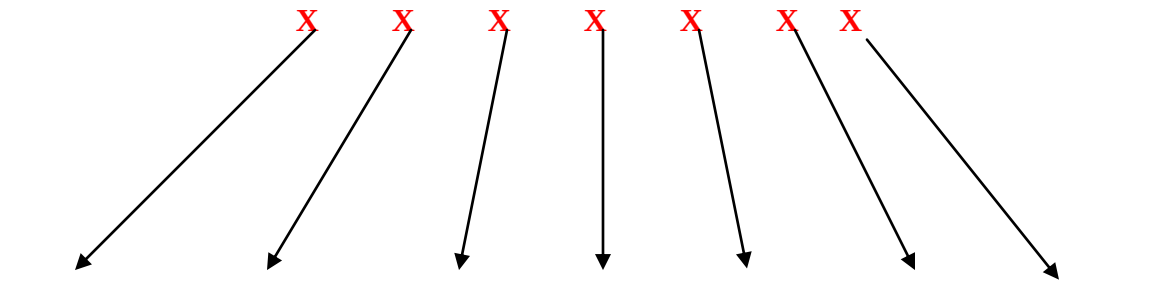

Figure 3.1. Nomenclature for test specimens.

3.2 Room Temperature Tests (ASTM D 3165 and ASTM D 1002)

ASTM D 3165 tests were conducted for six adhesives at room temperature (A, F, P, I, D, and H). The dimensions of the specimens, especially adhesive thickness, were measured before performing each test. The bondline thickness was measured using a stereoscope, as shown in Figure. 3.2. The goal of this test was to determine the shear strength of the joint and the Young's modulus of the adhesive from the test data (load-displacement) using FEM.

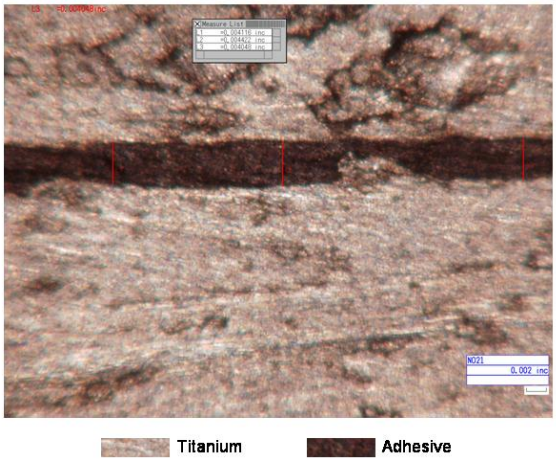

Figure 3.2. Measurement of adhesive thickness using stereoscope.

Usually the crosshead displacement (22 Kip MTS machine) was taken as the displacement data; however, since the adherend was titanium, which has high stiffness, a special arrangement was made to obtain the displacement data close to the overlap area. This arrangement included pasting laser extensometer reflective tapes near the shear area, as shown in Figure. 3.3. Also, the wedges of a mechanical extensometer were mounted on the other side of the specimen, exactly behind the location of reflective tapes, using clips, as shown in Figure 3.4. The test setup is shown in Figure 3.5.

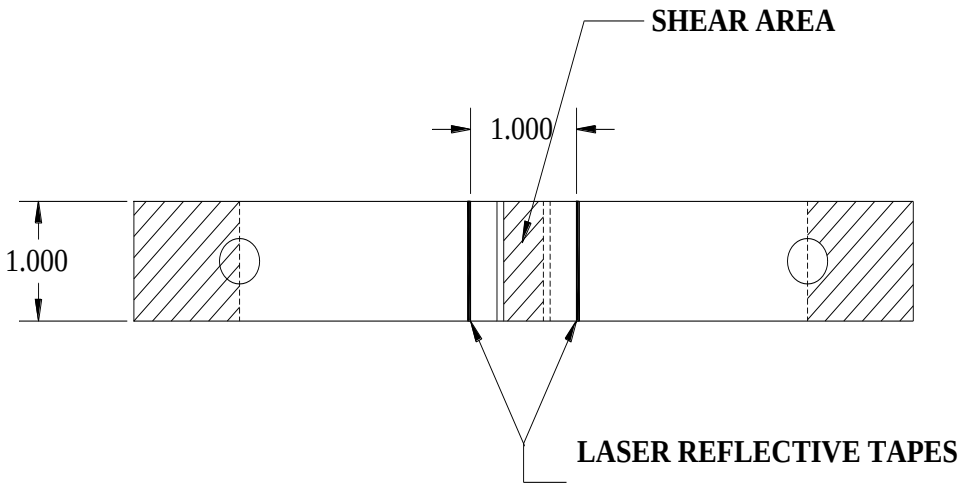

Figure 3.3. Location of laser extensometer reflective tapes on ASTM D 3165 specimen.

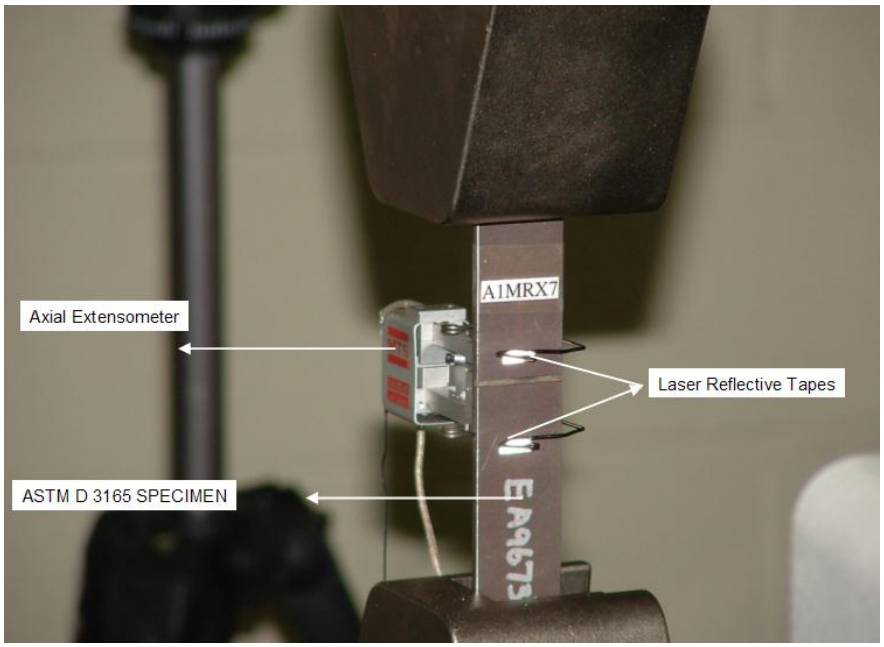

Figure 3.4. An ASTM D 3165 specimen where both mechanical extensometer and laser extensometer reflective tapes are attached.

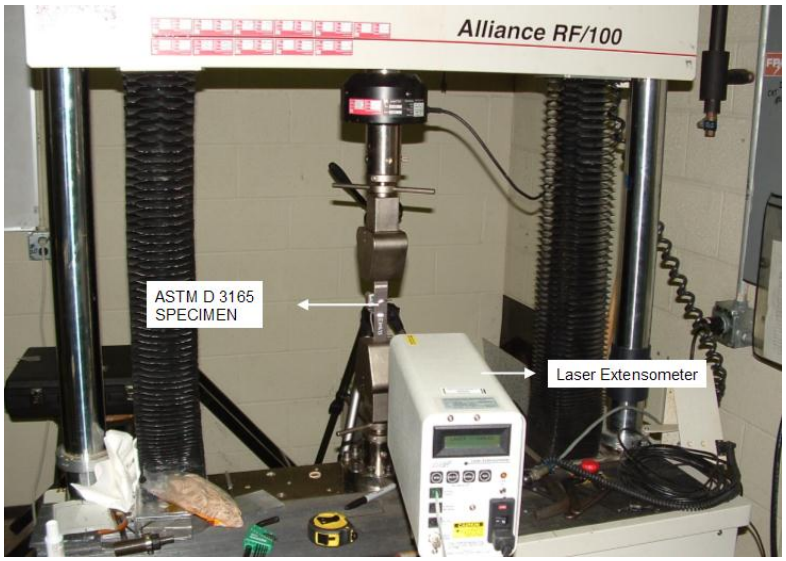

Figure 3.5. Test setup for ASTM D 3165 specimens (figure shows specimen along with laser extensometer).

Laser extensometers are used for strain measurement in materials testing. They are high precision non-contacting units. Details of a laser extensometer including its specifications are provided in Appendix C. In the laser extensometer, a high-speed laser scanner is used to measure the distance between reflective tape strips on the test specimen. The measurement range is from 0.3 inch to 3.2 inches and is determined by the person performing the test. The visible laser light is aimed at the specimen, where small reflective tape strips are set(glued to the specimen) at the desired gage length. The laser beams are subjected to fall on the specimen with a small inclination in the incident ray. Initially, when the rays strike the tapes, the extensometer displays the actual gage length. If desired, the zero buttons will offset the output to zero, so that the resultant reading during the test is just the elongation of the test specimen when the test is performed. The specifications of the laser extensometer used are given in Appendix C. The specimen was loaded up to failure, and the shear strength of the joint was determined by dividing the failure load by the overlap area.

Before the laser extensometer was used, it was calibrated to ensure the credibility of the data obtained. This arrangement is shown in Figure. 3.5. Two strips of laser reflecting tape were attached one inch apart, each of which was equidistant from the center of the specimen, as shown in Figure 3.3. At almost the same position, a mechanical extensometer was fixed behind the surface on which reflective tapes were pasted as shown in Figure. 3.4. Theoretically and practically the readings of laser extensometer and mechanical extensometer should be very close. While mounting the wedge of the mechanical extensometer may slip to the notch (slot) of the ASTM D 3165 specimens. Therefore, care must be taken while mounting the mechanical extensometer.

ASTM D 1002 tests to obtain the shear strength of the joint were conducted for five adhesives with different surface preparation, at room temperatures as shown in Figure 3.1. Adhesives tested were A, I, F, C, and H. Setups for this test were the same as for the ASTM D 3165 specimens, described previously; however, no extensometer of any kind was attached to the specimens because the goal was to obtain the shear strength of the joint which is simply but the failure load divided by the overlap area.

3.3 High-Temperature Tests

The temperatures at which the elevated temperature tests were conducted were 600ºF and 750ºF. Since the load cell of the testing machine shouldnot reach a temperature of more than 150ºF, enough room on the fixture was provided to cool it so that the heat flowing to the load cell could be prevented. Two types of furnaces were used for high-temperature testing: ATS 304 6/92 series 3160 split box furnace (Appendix D), and MTS 653 furnace (Appendix E). While using the ATS furnace, extra care was taken to cool the fixture. The test setup using the ATS furnace is shown in Figure 3.6.

The outer square tube was covered with a vacuum bag into which nitrogen was pumped. Tubes were properly arranged so that nitrogen flowed smoothly in and out of the vacuum bag. The square tube contained many holes in order to cool it properly**.**

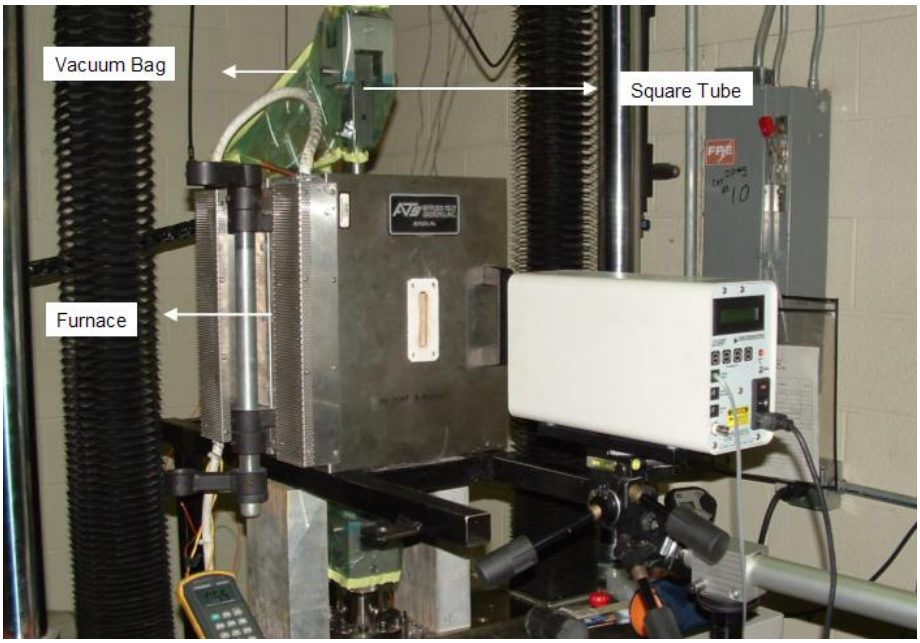

Figure 3.6. Test setup for elevated temperature tests using ATS furnace series 3160.

The high temperature was provided by an ATS (series 3160) split box furnace capable of temperatures as high as 2,200ºF. This series furnace is compatible with a variety of accessories, including thermocouples, controls, recording systems, view ports, mounting brackets, etc. The temperature profile, 600ºF rise in 15 minutes and then soaking it at 600ºF for 15 minutes, was programmed using the control panel of the furnace. The goal was to heat the specimen to 600ºF with a variation of ±10ºF. For this, a witness specimen was attached with a thermocouple in the overlap area near the real specimen, as shown in Figure 3.7. The thermocouple (J type) was then provided as an input to the control panel of the furnace, so that the temperature could be controlled based on the temperature of the witness specimen. It was found that the maximum temperature

difference between the real specimen and the witness specimen was 15ºF, i.e., when the temperature of the witness specimen reached 615ºF the temperature of the real specimen reached 600ºF. The maximum overshoot temperature of the witness specimen while running the profile (600ºF rise in 15 minutes and soak 600ºF for 15 minutes) was 616ºF, while at the same time, the temperature of the real specimen was 602ºF, which was within the allowable range of 600±10ºF. These conclusions were made during the trial runs where two specimens with thermocouples were kept in the position where the real and witness specimens were to be kept. The best profile achieved using ATS furnace is shown in Figure 3.8.

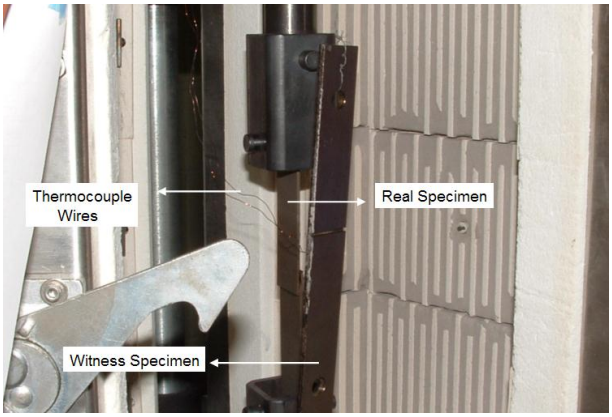

Figure 3.7. Inside view of the ATS furnace.

Based on the conclusion made from the trial runs, actual tests were conducted using the profile (600ºF in 15 minutes and soak the temperature 600ºF for 15 minutes), and the specimen mounted on the MTS machine (22 kip) was pulled when the profile ended after 30 minutes. The failure load was recorded for each specimen and the shear strength of each adhesive joint was determined at 600ºF. Tests conducted for both ASTM D 3165 and ASTM D 1002 specimens were similar.

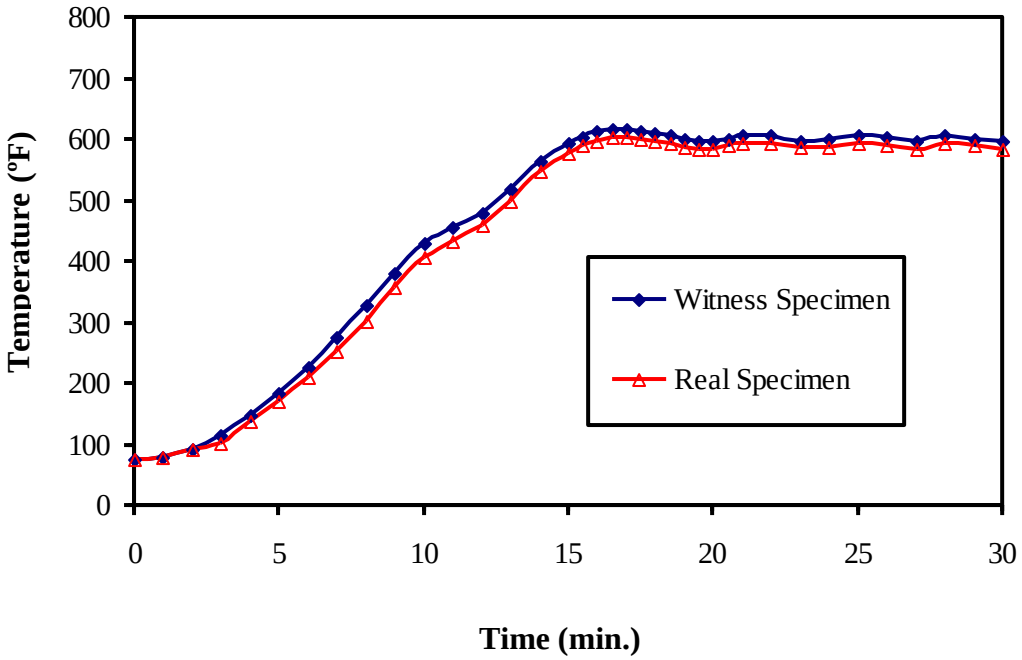

Figure 3.8. Temperature profile made using ATS furnace (600ºF rise in 15 min. and soak the temperature 600ºF for 15 min.).

Later on, 750ºF was used for the MTS 653 furnace. Trial runs were done to obtain the temperature difference of the oven and the specimen to determine the profile and set point temperature, which is programmed using the control panel of the furnace. This is done using a controller attached to the furnace. There was no need to attach a witness specimen because the distance between the furnace wall and the specimen was very small.

Many trial runs were performed using specimens with thermocouples in the overlap area to obtain the difference in temperature between the furnace wall and the specimen. The furnace wall temperature was recorded directly from the control panel, and it was determined that with the profile of 765^{o}F rise in 15 minutes and 765^{o}F dwell

for 15 minutes, the specimen reached the temperature of 750+6°F, as shown in Figure 3.9. The MTS 653 furnace had better control over the temperature than the ATS furnace, which is clear by comparing Figures 3.8 and 3.9. The MTS furnace had both lower- and upper-chamber thermocouples by which the temperatures were recorded and controlled. Here, the separation was removed and profiles run simultaneously. The test setup using the MTS 653 furnace is shown in Figure. 3.10.

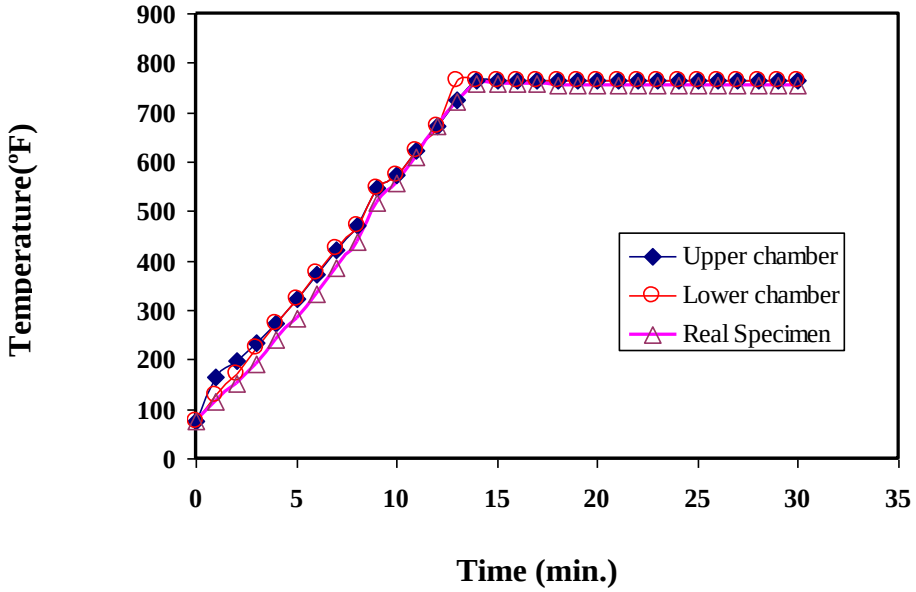

Figure 3.9. Temperature profile made using MTS furnace (750°F rise in 15 min. and soak the temperature 750°F for 15 min.).

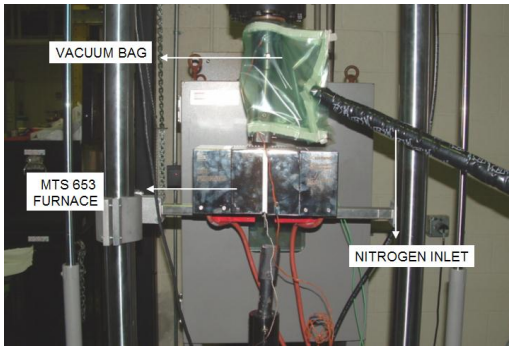

Figure 3.10. Test setup for 750°F tests using MTS 653 furnace.

3.4 Fixtures for ASTM D 5656 Specimens While Using Laser Extensometer

Figure 3.11 shows the fixtures for ASTM D 5656 specimens using the laser extensometer.

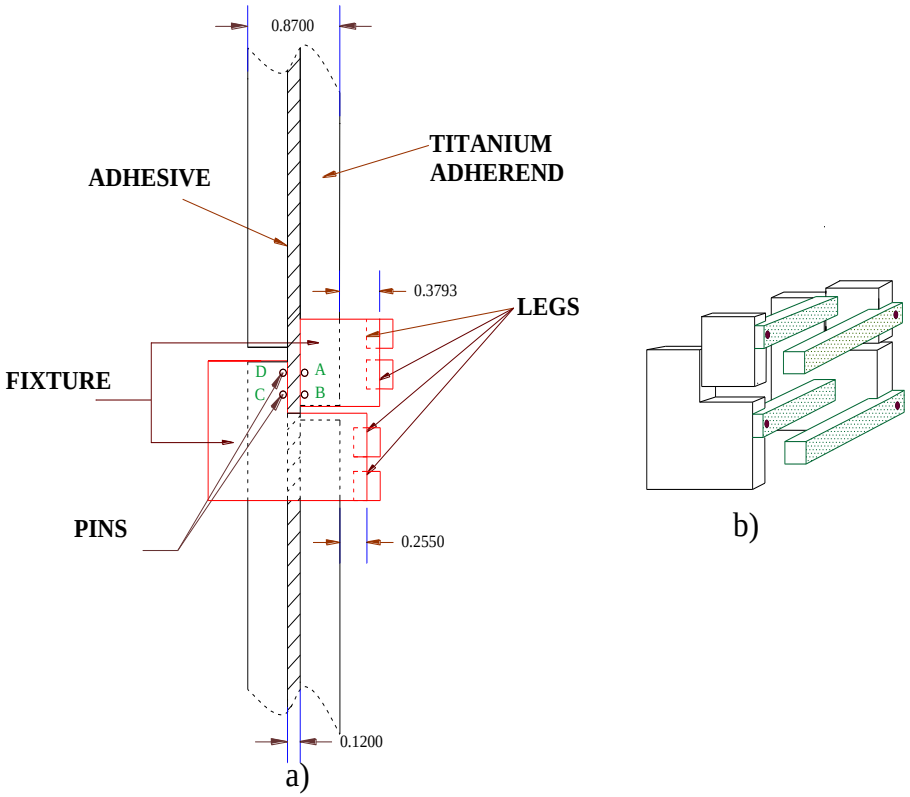

Figure 3.11. (a) Port/star side view of the fixtures for ASTM D 5656 specimen while using laser extensometer; (b) three-dimensional view of the whole fixture.

With respect to Figure 3.11, fixtures (part drawings are provided in Appendix F) were designed and machined at Wichita State University for measuring the displacements at locations A, B, C, and D while using the laser extensometer. These fixtures can be used to obtain the stress-strain properties of adhesives at room and elevated temperatures. At elevated temperatures, these fixtures are applicable only if there is a provision for a laser extensometer to scan the specimen through the furnace.

The design of the fixture was conceptualized by the location of the four holes on the ASTM D 5656 specimen and the direction of the laser scan as shown in Figure. 3.12. The fixtures on the port and star sides of the specimen consisted of rectangular and L-shaped blocks with pins, in order for the blocks to be directly be inserted into the holes on the specimen, as shown in Figure 3.13. These blocks were attached with legs on which the reflective tapes were mounted. It should be noticed that "legs" from every block come to the same face of the specimen, as shown in Figure 3.11(b) and Figure 3.13. When the ASTM D 5656 specimen is pulled, the fixtures that are attached to the holes of the specimen (A, B, C, and D on both sides, i.e., port and star) move with the holes. Therefore the linear displacements of the holes in the direction of load can be measured by using a laser extensometer and by mounting the reflective tapes on the legs of these fixtures, as shown in Figure 3.13.

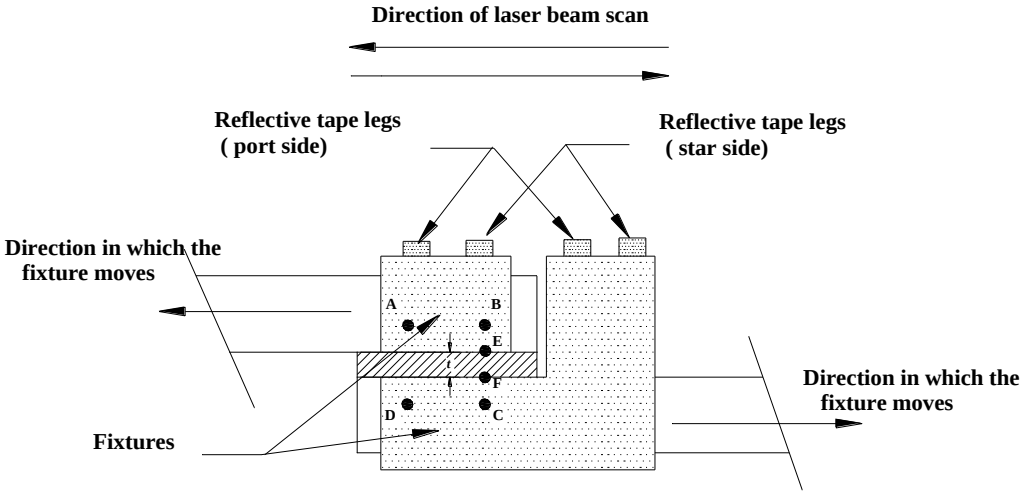

Figure 3.12. Detailed view of the center of the specimen with fixtures.

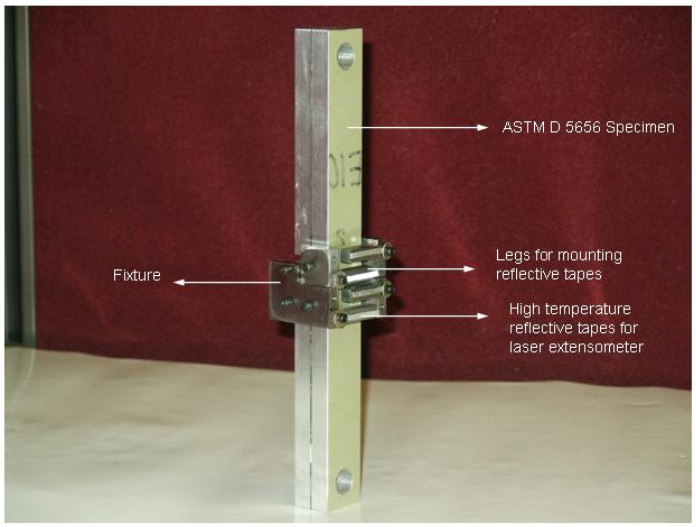

Figure 3.13. Fixtures mounted on ASTM D 5656 specimen while using laser extensometer.

By measuring the linear displacements of specimen holes with the laser extensometer, it is possible to determine the shear stress vs. shear strain relationship of the adhesive and thus calculate the shear modulus of the adhesive by including some correction factors along with the readings measured by the extensometer. The fixture designed is a modified version of the four-pin fixture designed by WSU, as shown in Figure. 2.9.

3.5 Finite Element Analysis of Adhesive Joints

ABAQUS 6.4-1 standard was used to analyze and simulate the ASTM D 3165 specimens tested at room temperature. Using ABAQUS, the ASTM D 3165 tests were simulated with different Young's moduli of adhesive. The adhesive Young's moduli that gave the same load-displacement data similar to the test data (laser extensometer and

mechanical extensometer) were determined. The modulus of adhesive that gave the same slope of the test data (load-displacement) was determined and finalized as the original Young's modulus of the adhesive. The finite element mesh of the ASTM D 3165 specimen is shown in Figure 3.14. Quadratic elements (CPE8R-plane strain eight-noded, reduced integration, quadrilateral elements with quadratic interpolation functions) were used to mesh both the adherend region and the adhesive regions. In the finite element mesh, nodes at the interface of adherend and adhesive were common to both regions.

The analyses were static plane strain. All nodes on the left end of the specimen were constrained in direction 1 (direction of load), the bottom nodes at both left and right ends were constrained in direction 2, and all nodes on the right end of the specimen were given displacement of 0.01inch in direction 1 so that the reaction load could be determined from the *.odb file (output database file). In Figure 3.14, two points, A and B, are represented and correspond to the reflective tapes of the laser extensometer that are one inch apart. The difference in displacements (displacement in direction 1 as shown in Figure 3.14) of points A and B and the summation of the reaction load of all nodes on the left end were determined from the history output data of the *.odb file of ABAQUS. Graphs were plotted with the readings of difference in displacements of points A and B on the *x*-axis and total reaction force on the *y*-axis at the same time intervals. This resulted in a load-displacement graph that was similar to that obtained from testing. If the slope of the load-displacement graph from testing matches with the slope of load-displacement graph obtained from FEM, then the value of Young's modulus for adhesive given in the input file (*.inp) of ABAQUS is the actual Young's modulus of the adhesive. However, all these comparisons were made when the graph was linear and the materials

were within the elastic range. The material properties of titanium were already determined from testing (E=16.9E6 and υ=0.39). If the slope didn't match, the ABAQUS input file was executed for a different Young's modulus of adhesive (the Poisson's ratio of the adhesive was fixed at 0.35). This process was repeated until the slope of both the graphs from FEM and test graphs matched. After this, the shear modulus of the adhesive was calculated from equation (3.1). The deformed shape of the element is shown in Figure 3.15. It can be noted from Figure 3.15 that the center region of the specimen rotates between the notches.

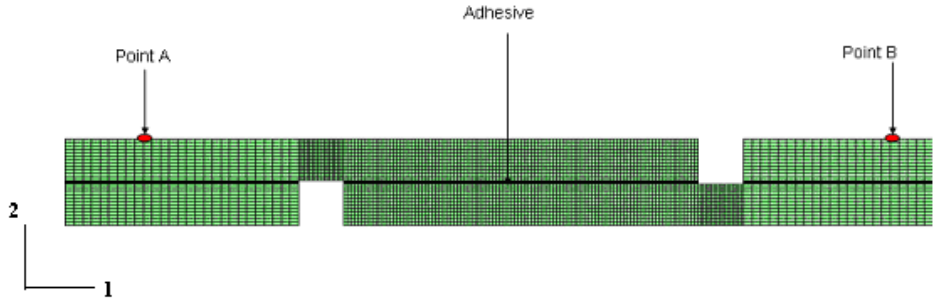

Figure 3.14. Finite element mesh of ASTM D 3165 specimen (center region).

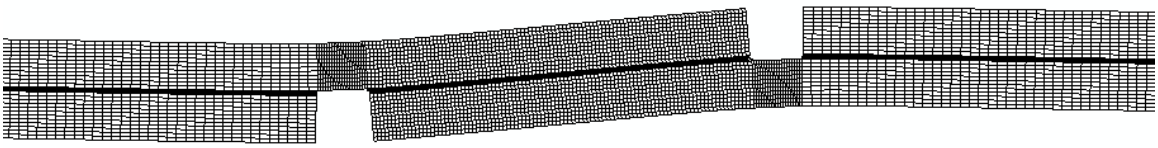

Figure 3.15. Deformed shape of the ASTM D 3165 specimen (center region).

The ABAQUS 6.4-1 standard was used to analyze ASTM D 5656 specimens at room temperature (considering only linear elastic properties). The primary objective of ASTM D 5656 test was to determine some of the significant mechanical properties, the stress-strain relationship and shear modulus of adhesives [14,19]. The test is performed by loading the thick adherend specimen, with the adhesive joint, at both ends. During this process, the relative displacements of the two adherends were measured using laser extensometer and the associated designed fixture (with four pins on one side, Figure 3.11), which was exclusively designed while using laser extensometer [14,19]. A better understanding about the mechanical behavior of joint was made using a two dimensional finite element model. This detailed analysis using finite element models helped to determine the correction factors that come up in calculating the shear modulus while using laser extensometer. Different finite element models were used for simulating specimens of different bondline thickness (0.001, 0.01, 0.04, 0.08 and 0.12 inch) [14,19]. Finite element analyses of the ASTM D5656 specimen models were performed to determine the correction factors involved in calculating the shear modulus of the adhesive using a laser extensometer for different adhesive shear moduli of 100, 150, 200 and 250 ksi. In all analyses, Poisson's ratio of the adhesive was assumed constant at 0.35. Based on this value and the shear moduli values, the Young's modulus values that were used during ABAQUS simulation were determined as

$$G = \frac{E}{2(1+\upsilon)} \tag{3.1}$$

where G is the shear modulus, υ is the Poisson's ratio, and E is the Young's modulus. The displacements of points A, B, C, D, E, and F were determined from FEM to formulate the correction factors while using a laser extensometer. The finite element

mesh and the boundary conditions of an ASTM D 5656 specimen are shown in Figure 3.16. Quadratic elements (CPE8R-plane strain eight-noded, reduced integration, quadrilateral element with quadratic interpolation functions) were used to mesh both the adherend region and the adhesive regions. Here also, the finite element model was done in such a way that the nodes at the interface of the adherend and adhesive were common to both regions. The center node of the adhesive on the left end of the specimen is constrained in directions 1, and 2, and the center node of the adhesive on the right end is constrained in direction 2. A concentrated load of 1,000 lbf was applied.

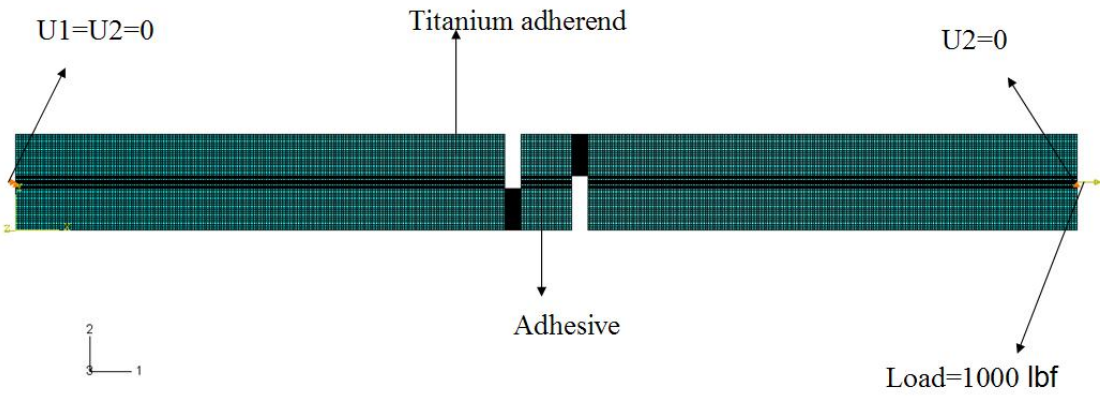

Figure 3.16. Finite element mesh of an ASTM D 5656 specimen with boundary conditions.

After the analyses were performed for models with different adhesive thicknesses and shear moduli, the displacements in directions 1 and 2 of points A, B, C, D, E, and F (A, B, C, and D which were at a distance of 0.042 inch from the adherend-adhesive interface), as shown in Figure 3.17, were recorded from the output file (*.odb) of ABAQUS.

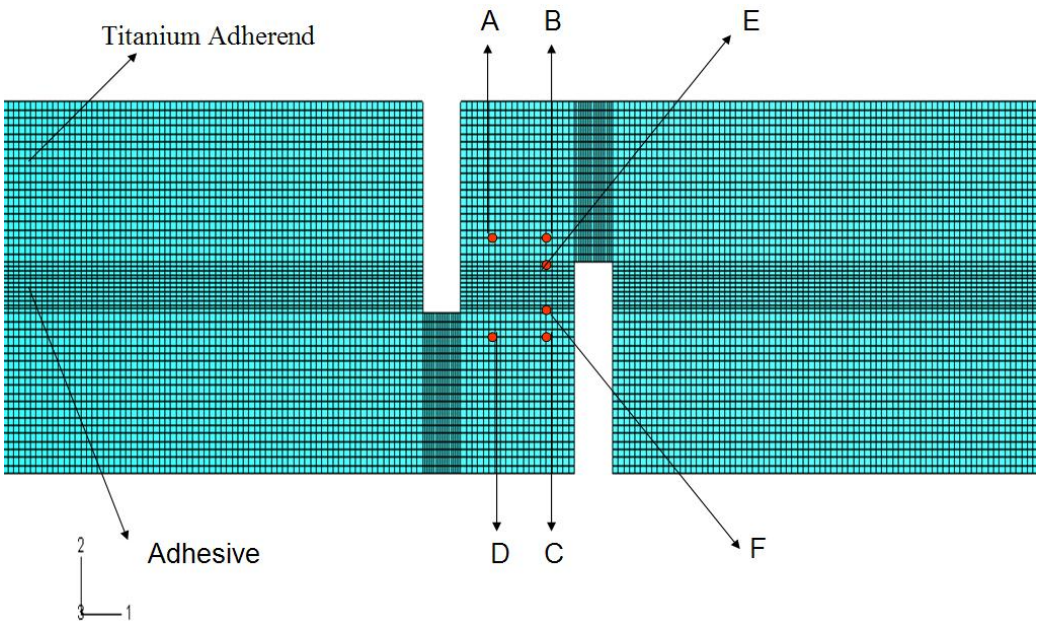

Figure 3.17. Locations of points (where the displacements were recorded).

CHAPTER 4

RESULTS AND DISCUSSIONS

4.1 Results of ASTM D 3165 and ASTM D 1002 Tests

All tests were conducted based on the ASTM standards, and the failure loads and failure modes, as shown in Figure 4.1, of the specimens were determined. For ASTM D 3165 specimens at room temperature, data from the laser extensometer and in some cases data from the mechanical extensometer were recorded and compared with the FEM model to determine the Young's modulus of the adhesive. This was done by comparing the slopes of the load-displacement graph obtained from the tests, i.e., the approximate slope of the laser extensometer readings in the elastic (linear region of the specimen) region were determined and compared to the FEM model, which gave the same slope as that of the testing data. The failure modes of the specimens were also analyzed after testing for both room temperature and elevated temperatures. For ASTM D1002 tests only, failure loads were necessary to determine the shear strength of adhesive joints. Figures 4.2 to 4.16 show the load-displacement curves from the laser and mechanical extensometers and slopes of all ASTM D 3165 specimens (Y-axis shows the load and X-axis shows the displacement). Specimens that do not specify the type of surface preparation are all anodized.

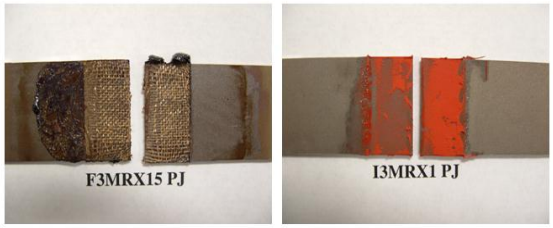

Figure 4.1. Pictures of the failed specimen.

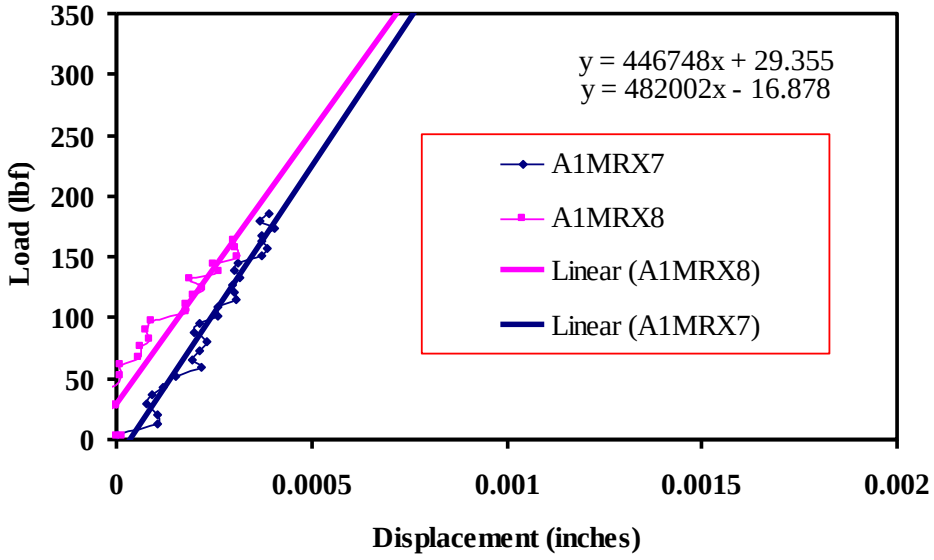

Figure 4.2. Laser extensometer readings of A1MRX7 and A1MRX8.

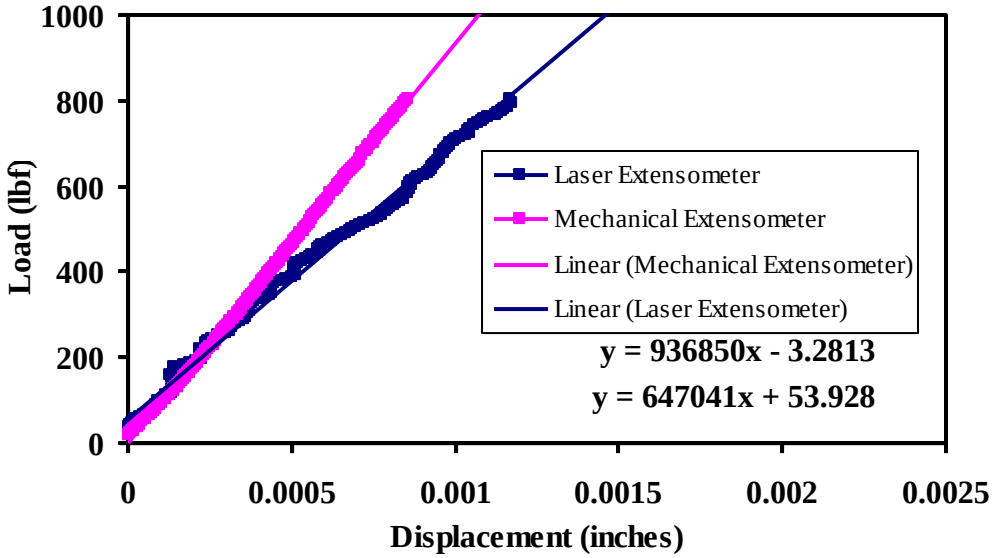

Figure 4.3. Extensometer readings of A1MRX12 PJ.

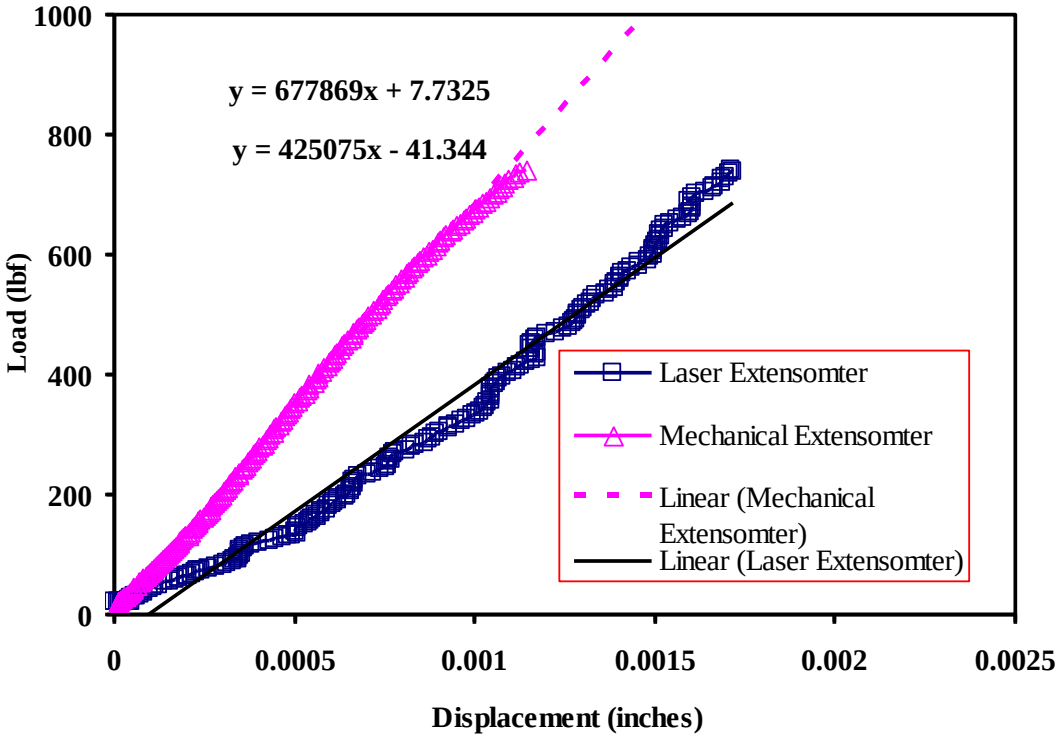

Figure 4.4. Extensometer readings of A1MRX13 PJ.

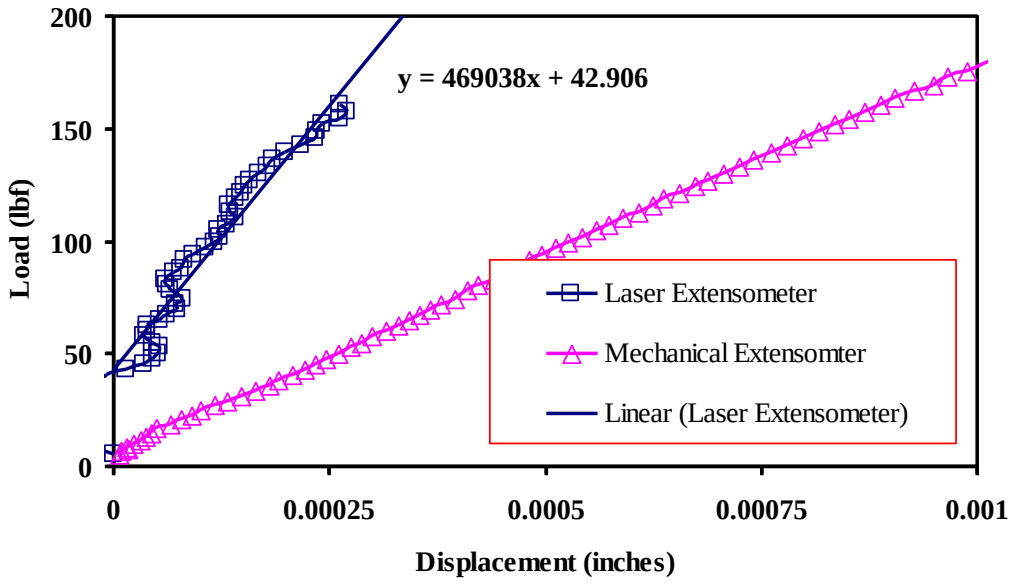

Figure 4.5. Extensometer readings of A1MRX16 AN.

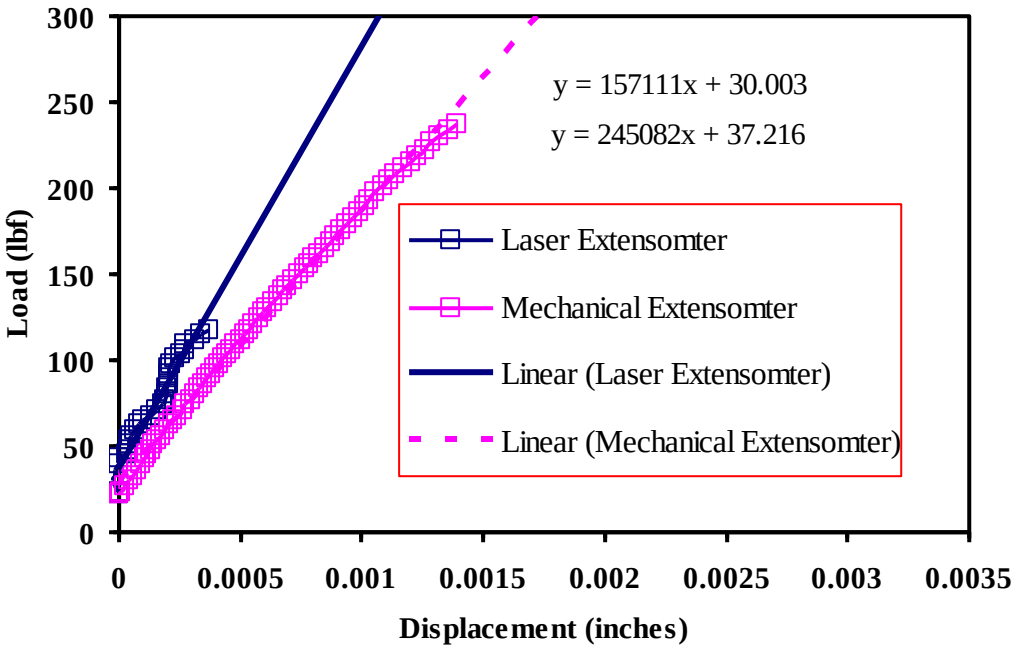

Figure 4.6. Extensometer readings of A1MRX17 AN.

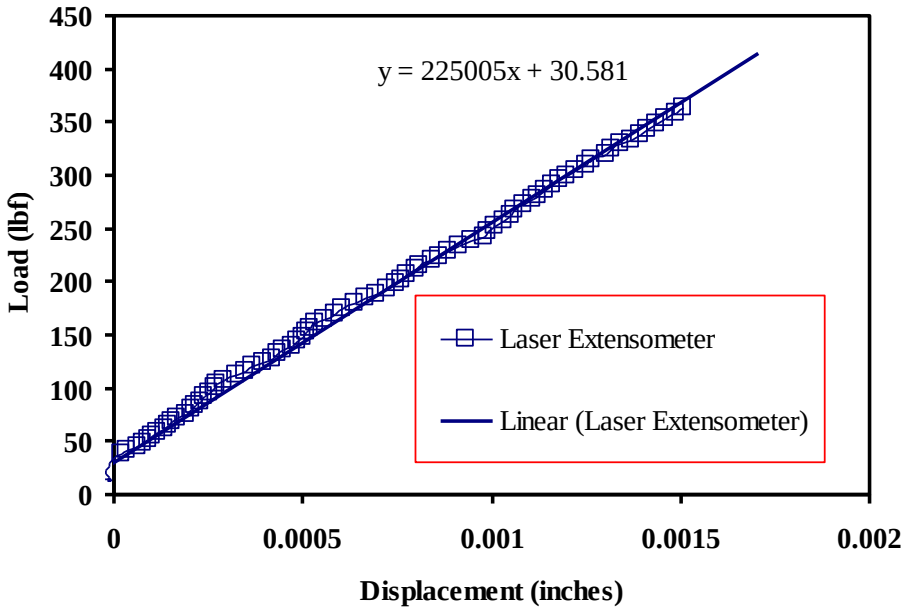

Figure 4.7. Laser extensometer readings of A1MRX4.

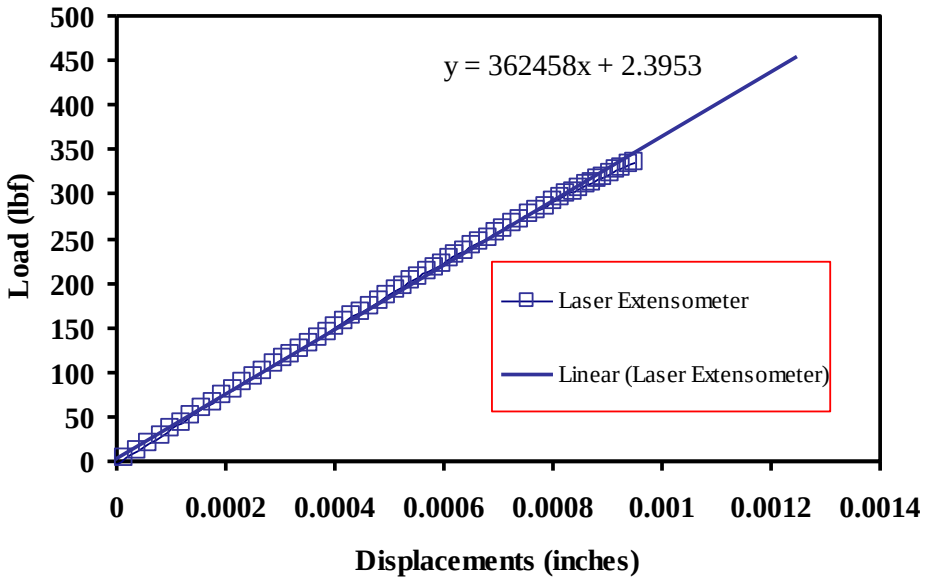

Figure 4.8. Laser extensometer readings of A1MRX5.

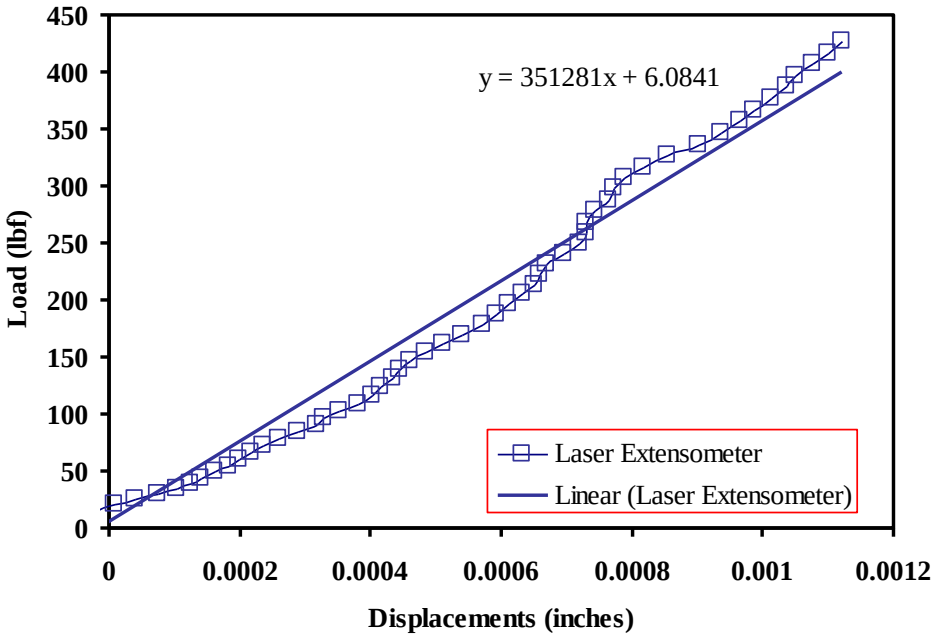

Figure 4.9. Laser extensometer readings of A1MRX6.

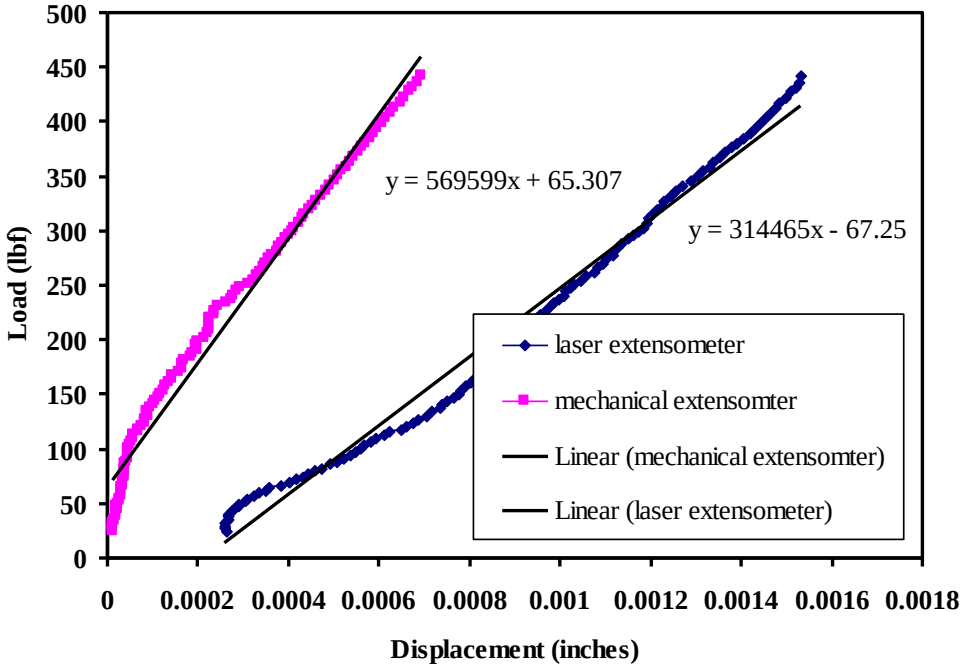

Figure 4.10. Extensometer readings of H1MRX1.

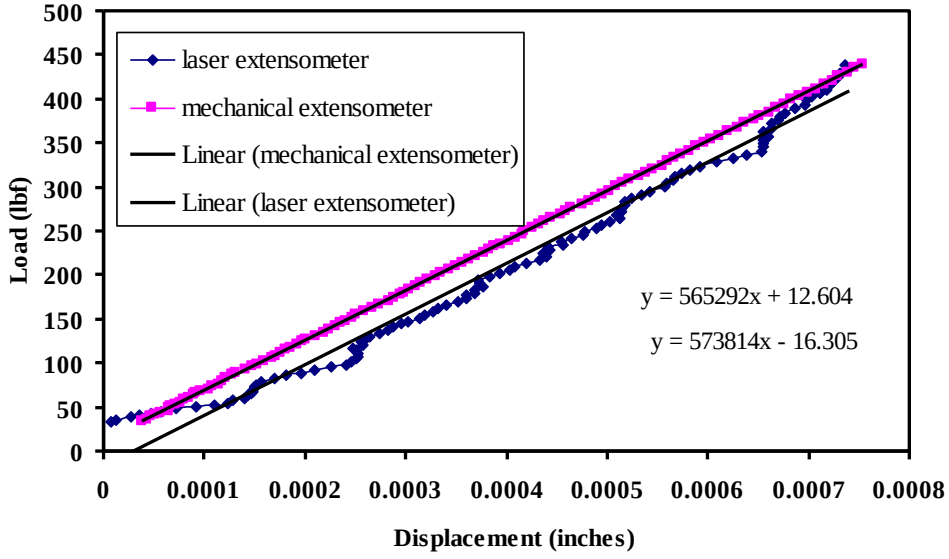

Figure 4.11. Extensometer readings of H1MRX3.

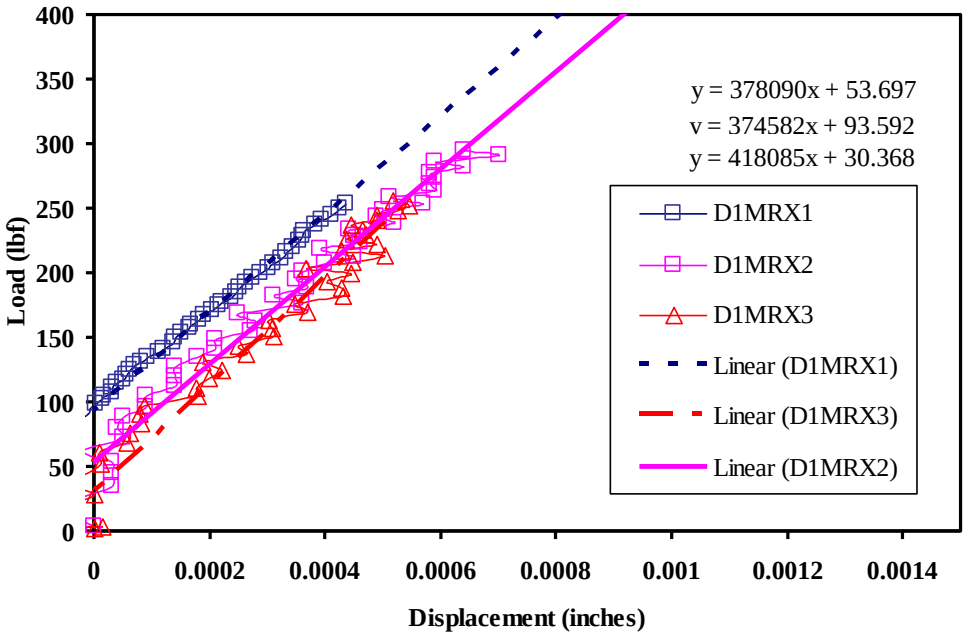

Figure 4.12. Laser extensometer readings of D1MRX1, D1MRX2 and D1MRX3.

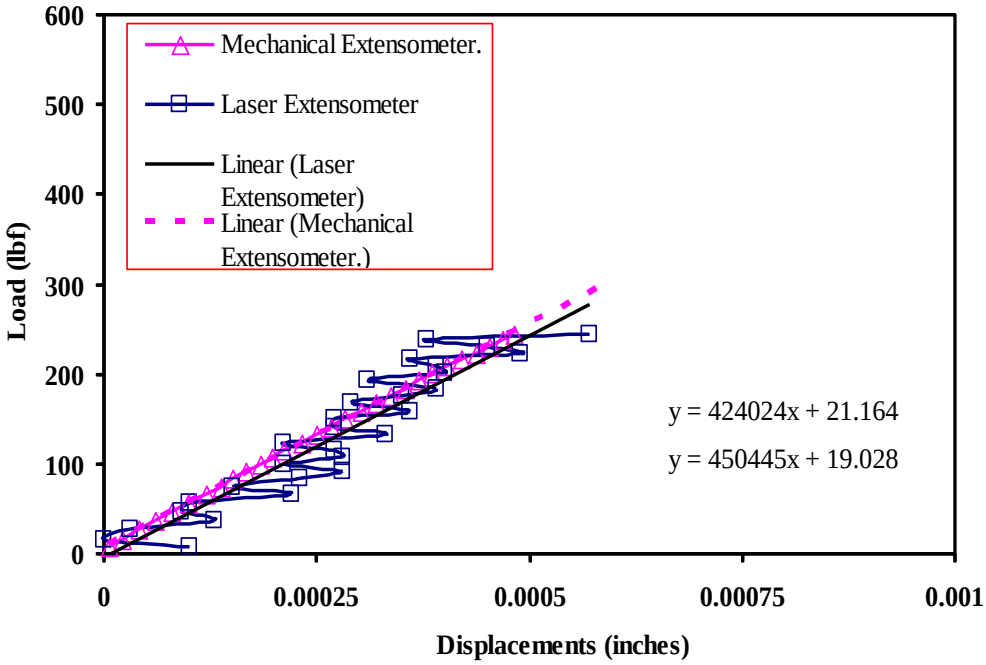

Figure 4.13. Extensometer readings of F1MRX1.

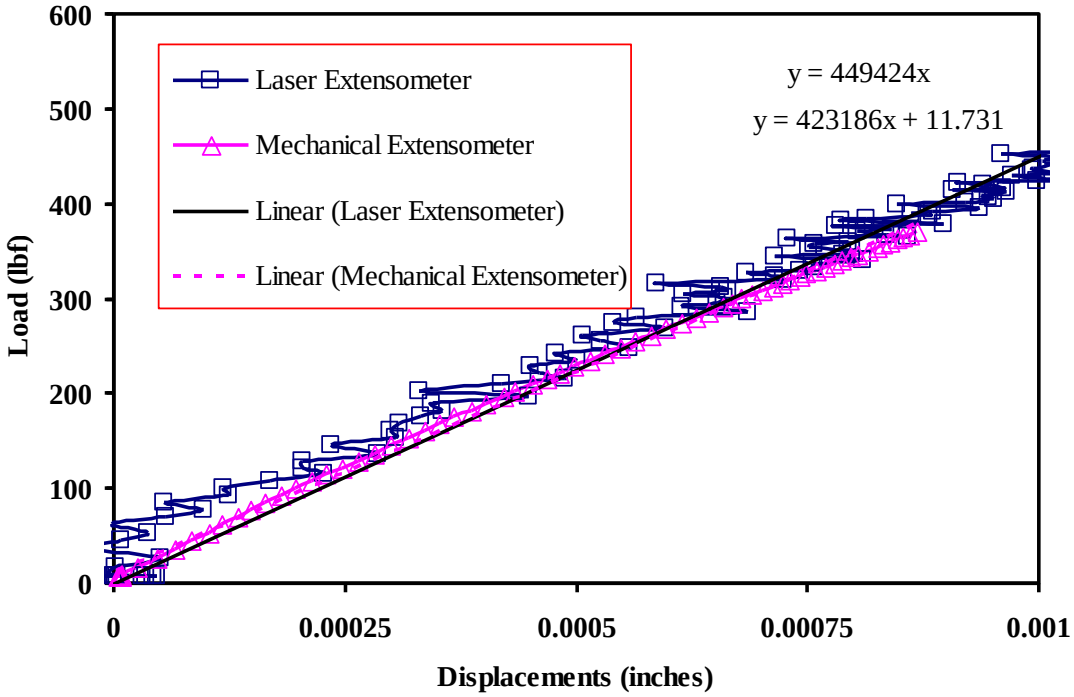

Figure 4.14. Extensometer readings of P1MRX1.

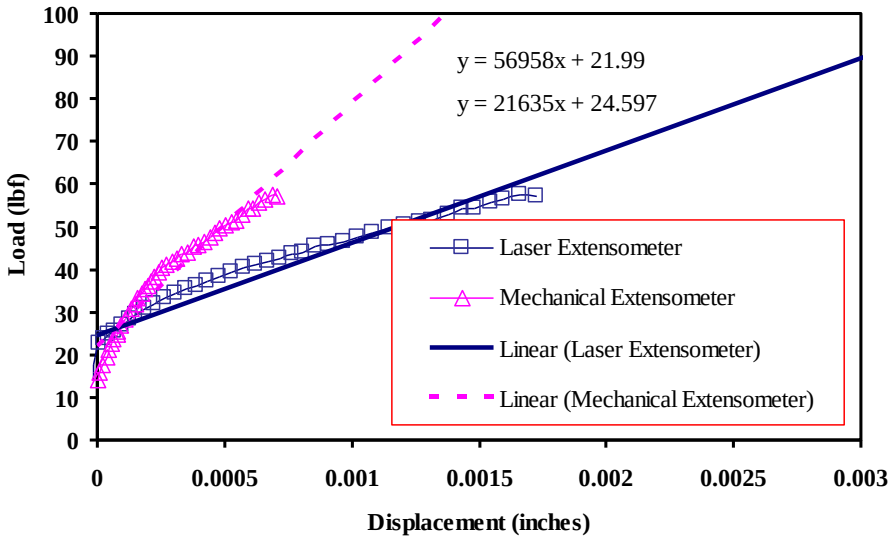

Figure 4.15. Extensometer readings of I1MRX1.

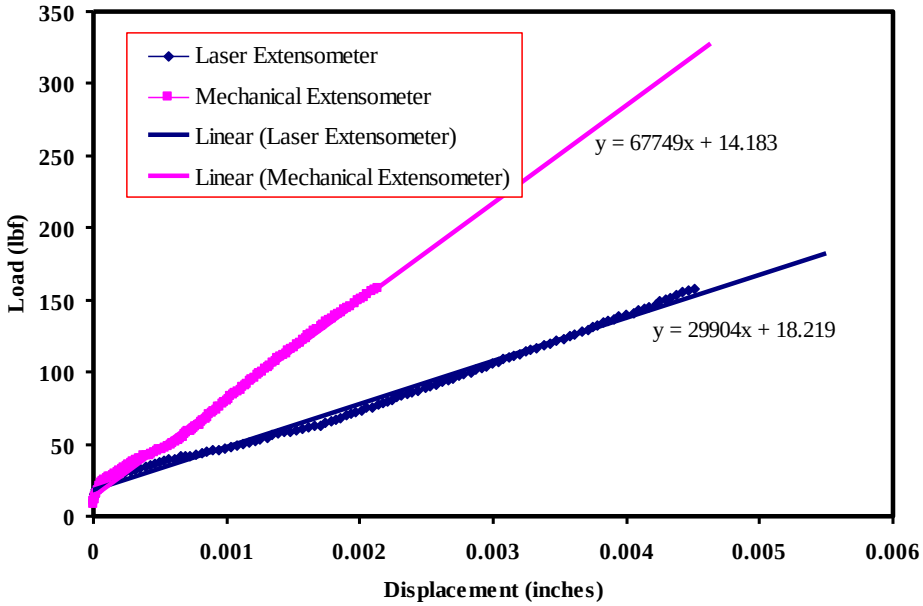

Figure 4.16. Extensometer reading of I1MRX2.

From finite element modeling using ABAQUS, load-displacement graphs were plotted and slopes were recorded for different Young's moduli of adhesives, as shown in Figure 4.17. In all tests, mechanical extensometer data also were recorded to ensure the accuracy of laser extensometer data. Comparison was made between the slope of the test data and that from FEM. Matching slopes, it meant that the Young's modulus of the adhesive used in the finite element model matched with the actual value used in the physical test. Some of the load displacement graphs from FEM are shown in Figure 4.17.

Each of these analyses was performed after measuring the dimensions of the specimens, especially the adhesive thickness. Tables 4.1 to 4.4 give detailed descriptions of the ASTM D 3165 specimen tested. Details of ASTM D 1002 specimens tested are shown in Tables 4.5 to 4.18.

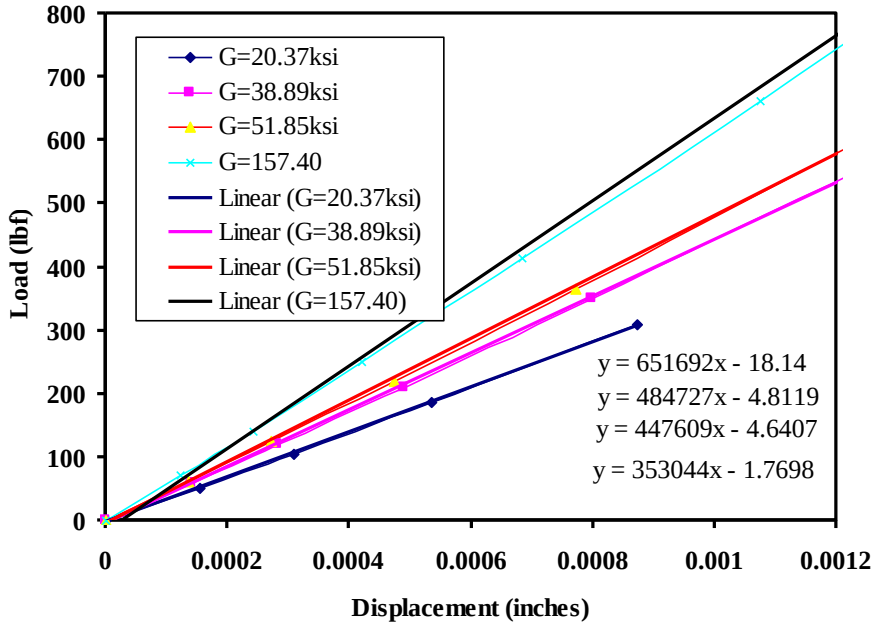

Figure 4.17. Load-displacement data and slope from FEM (ABAQUS 6.4).

In Tables 4.1 to 4.18 all dimensions regarding thickness, width, overlap length, notch size, specimen hole diameter, hole-to-hole distance, and thickness of adhesives are in inches, while failure load is in lbf, and shear modulus, G from FEM, is in ksi.

TABLE 4.1

ASTM D 3165 SPECIMENS WITH ADHESIVE A

SPECIMEN	A1MRX1	A1MRX2	A1MRX3	A1MRX4	A1MRX5	A1MRX6	A1MRX7
Total thickness (in.)							0.13
Width (in.)							0.997
Overlap length (in.)							0.506
Notch size (in.)							0.066
Hole diameter (in.)							0.374
Hole-hole distance (in.)							5.13
Thickness of adhesive (in.)							0.006
Failure load (lbf)	869	692	842	737	515	591	508.94
Extensometers Used	-	-	-	-	Both	Both	Both
Manufacture's 'E 'value (ksi)							
Slope of load-disp.(test) (lbf/in.)				#	362458	351281	482002
G from FEM (ksi)					22	20	50

TABLE 4.2

ASTM D 3165 SPECIMENS WITH ADHESIVE A

SPECIMEN	A1MRX8	A1MRX9	A1MRX12 PJ	A1MRX13 PJ	A1MRX16 AN	A1MRX17 AN
Total thickness (in.)	0.126	0.126				
Width (in.)	0.981	0.992				
Overlap length (in.)	0.485	0.513				
Notch size (in.)	0.064	0.065				
Hole diameter (in.)	0.373	0.373				
Hole-hole distance (in.)	5.12	5.14				
Thickness of adhesive (in.)	0.004	0.00597				
Failure load (lbf)	520.94	418	895	748	282	350
Extensometers Used	Both	Both	Both	Both	Both	Both
Manufacture's 'E 'value (ksi)						
Slope of load-disp.(test) (lbf/in.)	446748	#	647041	425075	469038	#
G from FEM (ksi)	39		143	33	46	

TABLE 4.3

ASTM D 3165 SPECIMENS WITH ADHESIVES F, P, AND I

SPECIMEN	F1MRX1	F1MRX2	F1MRX3	P1MRX1	I1MRX1	I1MRX2
Total thickness (in.)	0.1275	0.125	0.125	0.1275	0.124	0.12
Width (in.)	0.999	0.9975	1	1.001	1.004	0.998
Overlap length (in.)	0.51	0.51	0.51	0.5065	0.499	0.498
Notch size (in.)	0.064	0.065	0.63	0.064	0.067	0.067
Hole diameter (in.)	0.3755	0.375	0.375	0.375	0.373	0.366
Hole-hole distance (in.)	5	5.12	5.105	5	5.136	5.13
Thickness of adhesive (in.)	0.00349	0.00373	0.003412	0.00484	#	#
Failure load (lbf)	1081			986	210	207
Extensometers Used	Both			Both	Both	Both
Manufacture's 'E 'value (ksi)						
Slope of load-disp.(test) (lbf/in.)	424024			447751	20440	29904
G from FEM (ksi)	32			39	#	#

TABLE 4.4

ASTM D 3165 SPECIMENS WITH ADHESIVES D, AND H

SPECIMEN	D1MRX1	D1MRX2	D1MRX3	H1MRX1	H1MRX2	H1MRX3
Total thickness (in.)				0.126	0.125	0.125
Width (in.)				1.004	1.018	1.003
Overlap length (in.)				0.494	0.503	0.504
Notch size (in.)				0.061	0.064	0.062
Hole diameter (in.)				0.369	0.372	0.37
Hole-hole distance (in.)				5.114	5.128	5.12
Thickness of adhesive (in.)				0.00425	0.0038	0.00485
Failure load (lbf)	630.7	674.4	710	805	damaged	857
Extensometers Used	Both	Both	Both	Both		Both
Manufacture's 'E 'value (ksi)						
Slope of load-disp.(test) (lbf/in.)	374582	378090	418085	559204		541075
G from FEM (ksi)	23	23	32	93		83

TABLE 4.5

ASTM D 1002 SPECIMENS WITH ADHESIVE A

SPECIMEN	A3MRX1	A3MRX2	A3MRX3	A3MRX4 PJ	A3MRX5 PJ	A3MRX6 PJ
Adherend thickness (in.)	0.06	0.061	0.06	0.06	0.06	0.06
Total thickness (in.)	0.123	0.123	0.123	0.122	0.122	0.122
Overlap length (in.)	0.499	0.498	0.498	0.499	0.499	0.498
Width (in.)	1.002	1.002	1.002	1.002	1.002	1.002
Hole diameter (in.)	0.375	0.375	0.375	0.373	0.374	0.375
Hole-hole distance (in.)	5.138	5.139	5.137	5.153	5.145	5.148
Total length (in.)	7.5	7.5	7.5	7.5	7.5	7.5
Thickness of adhesive (in.)	#	#	#	#	#	#
Failure load (lbf)	1077.789	1060.103	1004.252	877.308	860.083	920.45
Fixture used	GRIP	GRIP	GRIP	GRIP	GRIP	GRIP
Date of Test	1/11/2005	1/11/2005	1/11/2005	1/11/2005	1/11/2005	1/11/2005

TABLE 4.6

ASTM D 1002 SPECIMENS WITH ADHESIVE A

SPECIMEN	A3MRX1 PJ	A3MRX2 PJ	A3MRX3 PJ	A3MEX1 PJ at 600ºF	A3MEX2 PJ at 600ºF	A3MEX3 PJ at 600ºF
Adherend thickness (in.)	0.06	0.06	0.06	0.06	0.06	0.06
Total thickness (in.)	0.123	0.123	0.122	0.122	0.123	0.122
Overlap length (in.)	0.499	0.498	0.499	0.499	0.498	0.499
Width (in.)	1.002	1.002	1.002	0.999	1.002	1.002
Hole diameter (in.)	0.375	0.375	0.373	0.375	0.375	0.373
Hole-hole distance (in.)	5.138	5.137	5.153	5.138	5.137	5.153
Total length (in.)	7.5	7.5	7.5	7.5	7.5	7.5
Thickness of adhesive (in.)	#	#	#	#	#	#
Failure load (lbf)	634.283	635.487	597.16	74.046	105.888	118.342
Fixture used	PIN	PIN	PIN	PIN	PIN	PIN
Date of Test	4/25/2005	4/25/2005	4/25/2005	5/12/2005	5/12/2005	5/12/2005

TABLE 4.7

ASTM D 1002 SPECIMENS WITH ADHESIVE H

SPECIMEN	H3MRX1 PJ	H3MRX2 PJ	H3MRX3 PJ	H3MEX1 PJ at 600°F	H3MEX2 PJ at 600°F	H3MEX3 PJ at 600°F
Adherend thickness (in.)	0.06	0.06	0.06	0.06	0.06	0.06
Total thickness (in.)	0.122	0.122	0.122	0.122	0.122	0.122
Overlap length (in.)	0.499	0.499	0.498	0.5	0.498	0.499
Width (in.)	1.002	1.002	1.002	0.996	1.002	1.002
Hole diameter (in.)	0.373	0.374	0.375	0.377	0.375	0.374
Hole-hole distance (in.)	5.153	5.145	5.148	5.139	5.148	5.145
Total length (in.)	7.5	7.5	7.5	7.49	7.5	7.5
Thickness of adhesive (in.)	#	#	#	#	#	#
Failure load (lbf)	1154.115	1028	1229.79	536.988	490.117	527.557
Fixture used	PIN	PIN	PIN	PIN	PIN	PIN
Date of Test	4/25/2005	4/25/2005	4/25/2005	5/9/2005	5/9/2005	5/9/2005

TABLE 4.8

ASTM D 1002 SPECIMENS WITH ADHESIVE I

SPECIMEN	I3MRX1 PJ	I3MRX2 PJ	I3MRX3 PJ	I3MEX1 PJ at 600°F	I3MEX2 PJ at 600°F	I3MEX2 PJ at 600°F
Adherend thickness (in.)	0.06	0.06	0.06	0.06	0.06	0.06
Total thickness (in.)	0.122	0.122	0.122	0.122	0.122	0.122
Overlap length (in.)	0.499	0.499	0.499	0.499	0.489	0.51
Width (in.)	1.002	1.002	0.998	1.002	0.998	1.001
Hole diameter (in.)	0.373	0.376	0.373	0.373	0.373	0.373
Hole-hole distance (in.)	5.153	5.16	5.153	5.153	5.142	5.152
Total length (in.)	7.51	7.51	7.52	7.51	7.51	7.51
Thickness of adhesive (in.)	#	#	#	#	#	#
Failure load (lbf)	99.5	98.285	94.89	18.41	27.5	23.625
Fixture used	PIN	PIN	PIN	PIN	PIN	PIN
Date of Test	5/5/2005	5/5/2005	5/5/2005	5/6/2005	5/6/2005	5/6/2005

TABLE 4.9

ASTM D 1002 SPECIMENS WITH ADHESIVE C

SPECIMEN	C3MRX1	C3MRX2	C3MRX3	C3MRX1 PJ	C3MRX2 PJ	C3MRX3 PJ
Adherend thickness (in.)	0.058	0.058	0.057	0.058	0.058	0.061
Total thickness (in.)	0.122	0.123	0.122	0.123	0.125	0.125
Overlap length (in.)	0.512	0.491	0.495	0.489	0.497	0.5
Width (in.)	1	0.999	0.997	0.996	0.996	1.002
Hole diameter (in.)	0.375	0.373	0.37	0.377	0.377	0.376
Hole-hole distance (in.)	5.134	5.143	5.148	5.154	5.167	5.154
Total length (in.)	7.512	7.513	7.532	7.522	7.523	7.521
Thickness of adhesive (in.)	#	#	#	#	#	#
Failure load (lbf)	1250.048	1352.806	1345.672	1373.6	1385.6	1359.6
Fixture used	PIN	PIN	PIN	PIN	PIN	PIN
Date of Test	2/23/2005	2/23/2005	2/23/2005	3/4/2005	3/4/2005	3/4/2005

TABLE 4.10

ASTM D 1002 SPECIMENS WITH ADHESIVE C

SPECIMEN	C3MRX7 PJ	C3MRX8 PJ	C3MRX9 PJ	C3MEX7 PJ at 600ºF	C3MEX8 PJ at 600ºF	C3MEX9 PJ at 600ºF
Adherend thickness (in.)	0.058	0.057	0.058	0.06	0.057	0.06
Total thickness (in.)	0.125	0.125	0.125	0.125	0.124	0.124
Overlap length (in.)	0.497	0.499	0.497	0.51	0.51	0.51
Width (in.)	0.996	0.999	0.996	1	1	1
Hole diameter (in.)	0.377	0.377	0.377	0.377	0.378	0.378
Hole-hole distance (in.)	5.167	5.168	5.166	5.142	5.14	5.142
Total length (in.)	7.523	7.525	7.524	7.51	7.5	7.51
Thickness of adhesive (in.)	#	#	#	#	#	#
Failure load (lbf)	1101.47	1101.76	928.99	788.657	802.42	844.24
Fixture used	PIN	PIN	PIN	PIN	PIN	PIN
Date of Test	5/5/2005	5/5/2005	5/5/2005	5/6/2005	5/6/2005	5/6/2005

TABLE 4.11

ASTM D 1002 SPECIMENS WITH ADHESIVE C

SPECIMEN	C3MEX1 at 600ºF	C3MEX2 at 600ºF	C3MEX3 at 600ºF	C3MEX1 PJ at 600ºF	C3MEX2 PJ at 600ºF	C3MEX3 PJ at 600ºF
Adherend thickness (in.)	0.06	0.06	0.06	0.06	0.06	0.06
Total thickness (in.)	0.123	0.124	0.123	0.124	0.124	0.123
Overlap length (in.)	0.519	0.5	0.51	0.512	0.51	0.51
Width (in.)	1.001	0.998	1.001	0.996	1	1.001
Hole diameter (in.)	0.377	0.377	0.378	0.377	0.378	0.378
Hole-hole distance (in.)	5.142	5.142	5.14	5.14	5.142	5.14
Total length (in.)	7.51	7.49	7.51	7.5	7.51	7.51
Thickness of adhesive (in.)	#	#	#	#	#	#
Failure load (lbf)	243.6	256.7	260.9	220.8	195.17	283.858
Fixture used	PIN	PIN	PIN	PIN	PIN	PIN
Date of Test	3/8/2005	3/4/2005	3/8/2005	3/8/2005	3/8/2005	3/8/2005

TABLE 4.12

ASTM D 1002 SPECIMENS WITH ADHESIVE F

SPECIMEN	F3MRX1 AN	F3MRX2 AN	F3MRX3 AN	F3MRX1 PJ	F3MRX2 PJ	F3MRX3 PJ
Adherend thickness (in.)	0.06	0.06	0.06	0.06	0.06	0.061
Total thickness (in.)	0.124	0.124	0.125	0.122	0.122	0.123
Overlap length (in.)	0.505	0.51	0.51	0.5	0.5	0.51
Width (in.)	0.996	0.998	0.996	0.996	0.996	0.996
Hole diameter (in.)	0.377	0.378	0.377	0.377	0.377	0.377
Hole-hole distance (in.)	5.14	5.145	5.143	5.143	5.139	5.14
Total length (in.)	7.5	7.51	7.521	7.498	7.49	7.49
Thickness of adhesive (in.)	#	#	#	#	#	#
Failure load (lbf)	1911.489	1866.9	1974.2	2094.4	2193	2406
Fixture used	PIN	PIN	PIN	PIN	PIN	PIN
Date of Test	3/4/2005	3/4/2005	3/4/2005	3/4/2005	3/4/2005	3/4/2005

TABLE 4.13

ASTM D 1002 SPECIMENS WITH ADHESIVE F

SPECIMEN	F3MEX1 AN at 600ºF	F3MEX2 AN at 600ºF	F3MEX3 AN at 600ºF	F3MEX1 PJ at 600ºF	F3MEX2 PJ at 600ºF	F3MEX3 PJ at 600ºF
Adherend thickness (in.)	0.061	0.06	0.06	0.06	0.06	0.06
Total thickness (in.)	0.125	0.124	0.125	0.122	0.124	0.123
Overlap length (in.)	0.5	0.5	0.51	0.5	0.51	0.51
Width (in.)	1.002	0.998	0.996	0.996	1	1.001
Hole diameter (in.)	0.376	0.377	0.377	0.377	0.378	0.378
Hole-hole distance (in.)	5.154	5.142	5.143	5.139	5.142	5.14
Total length (in.)	7.521	7.49	7.521	7.49	7.51	7.51
Thickness of adhesive (in.)	#	#	#	#	#	#
Failure load (lbf)	63.64	75.19	65.15	94.27	87.73	278.04
Fixture used	PIN	PIN	PIN	PIN	PIN	PIN
Date of Test	3/18/2005	3/18/2005	3/18/2005	3/18/2005	3/18/2005	3/18/2005

TABLE 4.14

ASTM D 1002 SPECIMENS WITH ADHESIVE F

SPECIMEN	F3MRX7 PJ	F3MRX8 PJ	F3MRX9 PJ	F3MRX13 PJ	F3MRX14 PJ	F3MRX15 PJ
Adherend thickness (in.)	0.06	0.061	0.06	0.06	0.061	0.061
Total thickness (in.)	0.123	0.123	0.123	0.122	0.123	0.123
Overlap length (in.)	0.499	0.498	0.498	0.5	0.51	0.498
Width (in.)	1.002	1.002	1.002	0.996	0.996	1.002
Hole diameter (in.)	0.375	0.375	0.375	0.377	0.377	0.375
Hole-hole distance (in.)	5.138	5.139	5.137	5.139	5.14	5.139
Total length (in.)	7.5	7.5	7.5	7.49	7.49	7.5
Thickness of adhesive (in.)	#	#	#	#	#	#
Failure load (lbf)	1803.328	1736.12	1850.23	2289.91	2069.912	1954.09
Fixture used	PIN	PIN	PIN	PIN	PIN	PIN
Date of Test	4/25/2005	4/25/2005	4/25/2005	5/5/2005	5/5/2005	5/5/2005

TABLE 4.15

ASTM D 1002 SPECIMENS WITH ADHESIVE F

SPECIMEN	F3MEX13 PJ at 600ºF	F3MEX14 PJ at 600ºF	F3MEX15 PJ at 600ºF	F3MRX7 PJ	F3MRX8 PJ	F3MRX9 PJ
Adherend thickness (in.)	0.06	0.06	0.06	0.06	0.061	0.06
Total thickness (in.)	0.122	0.124	0.123	0.123	0.123	0.123
Overlap length (in.)	0.5	0.51	0.51	0.499	0.498	0.498
Width (in.)	0.996	1	1.001	1.002	1.002	1.002
Hole diameter (in.)	0.377	0.378	0.378	0.375	0.375	0.375
Hole-hole distance (in.)	5.139	5.142	5.14	5.138	5.139	5.137
Total length (in.)	7.49	7.51	7.51	7.5	7.5	7.5
Thickness of adhesive (in.)	#	#	#	#	#	#
Failure load (lbf)	114.943	81.099	97.023	103.97	126.156	124.554
Fixture used	PIN	PIN	PIN	PIN	PIN	PIN
Date of Test	5/9/2005	5/9/2005	5/9/2005	5/11/2005	5/11/2005	5/11/2005

TABLE 4.16

ASTM D 1002 SPECIMENS WITH ADHESIVE F

SPECIMEN	F3MEX10 PJ at 600ºF	F3MEX11 PJ at 600ºF	F3MEX12 PJ at 600ºF	F3MEX4 AN at 600ºF	F3MEX5 AN at 600ºF	F3MEX6 AN at 600ºF
Adherend thickness (in.)	0.06	0.06	0.06	0.061	0.06	0.06
Total thickness (in.)	0.125	0.122	0.123	0.125	0.124	0.125
Overlap length (in.)	0.51	0.5	0.51	0.5	0.5	0.51
Width (in.)	0.996	0.996	1.001	1.002	0.998	0.996
Hole diameter (in.)	0.377	0.377	0.378	0.376	0.377	0.377
Hole-hole distance (in.)	5.143	5.139	5.14	5.154	5.142	5.143
Total length (in.)	7.521	7.49	7.51	7.521	7.49	7.521
Thickness of adhesive (in.)	#	#	#	#	#	#
Failure load (lbf)	121.799	122.412	135.91	71.4	97.36	99.25
Fixture used	PIN	PIN	PIN	PIN	PIN	PIN
Date of Test	7/13/2005	7/13/2005	7/13/2005	7/13/2005	7/13/2005	7/13/2005

TABLE 4.17

ASTM D 1002 SPECIMENS WITH ADHESIVE A, AND H

Specimen	A3MEX4 PJ at 750ºF	A3MEX5 PJ at 750ºF	A3MEX6 PJ at 750ºF	H3MEX5 PJ at 750ºF	H3MEX6 PJ at 750ºF
Failure load (lbf)	150.63	138.19	140.24	279.9	320.58
Fixture used	PIN	PIN	PIN	PIN	PIN
Date of Test	10/27/2005	10/27/2005	10/28/2005	10/27/2005	10/27/2005

TABLE 4.18

ASTM D 1002 SPECIMENS WITH ADHESIVE C, I, AND F

Specimen	C3MEX11 PJ at 750ºF	C3MEX12 PJ at 750ºF	I3MEX4 PJ at 750ºF	F3MEX16 PJ at 750ºF
Failure load (lbf)	232.3	224.58	7.88	74.4
Fixture used	PIN	PIN	PIN	PIN
Date of Test	10/27/2005	10/27/2005	10/28/2005	10/13/2005

4.2 Determining the Shear Modulus of Adhesive in ASTM D 5656 Tests Using Laser Extensometer

Various test methods were developed to test the structural adhesives in thin-film geometries. Among those, the ASTM D 5656 is used frequently to determine the shear properties of adhesives. During the test, some errors will be introduced if corrections are not made. These errors can occur due to: (1) Non-uniformity of adhesive shear stress distribution within the joint through both bondedline thickness and overlap length and (2) the measurement method by laser extensometer. A finite element analysis was conducted in order to simulate the mechanical behavior of the ASTM D 5656 specimen. In this case, for the specimens, the adherends used were made of titanium.

4.2.1 ASTM D 5656 Measurement and Analysis

During the physical test using the current KGR-1 type extensometers, it was difficult to obtain the displacement measurements from points E and F, which are located at the adherend/adhesive interface, as shown in Figure 4.18, because holes could not be drilled on points E and F. Hence, measurements were recorded from two nearby points, B, and C, as shown in Figure 4.18, at a distance of 0.042 inch from the adhesive-titanium interface so that the pins of the fixture could be inserted.

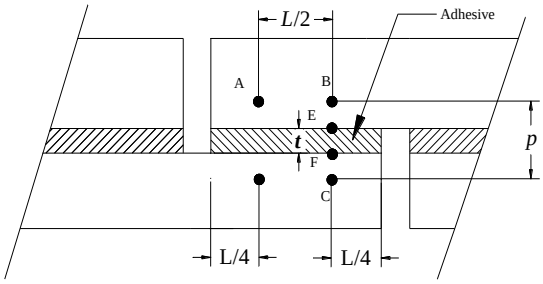

Figure 4.18. Symbols on the overlap region of ASTM D 5656 specimen.

G_{ASTM} [17], which is the shear modulus of the adhesive, determined by the test procedures of ASTM D 5656, is given by

$$G_{ASTM} = \frac{\tau_{average}}{\gamma_{apparent}} \tag{4.1}$$

where $\tau_{average}$ is the "apparent" or average shear stress of the adhesive and $\gamma_{apparent}$ is the "apparent" shear strain on the adhesive. The "apparent" or average shear stress, $\tau_{average}$, is calculated by

$$\tau_{average} = \frac{P}{Lb} \tag{4.2}$$

where P is the load applied on the specimen (which is 1,000 lbf), L is the length of overlap (the distance between two notches on the specimen, as shown in Figure 4.18), and b is the width of the specimen. Figure 4.18 shows the various symbols represented on the specimen, where t is the distance between E and F, which is the adhesive thickness, and p is the distance between B and C. In the ASTM D 5656 test, adherends in the overlap area rotate due to the eccentric load transfer via the adhesive/adherend interfaces. The rotation of the overlap region and the various coordinate systems are shown in Figure 4.19.

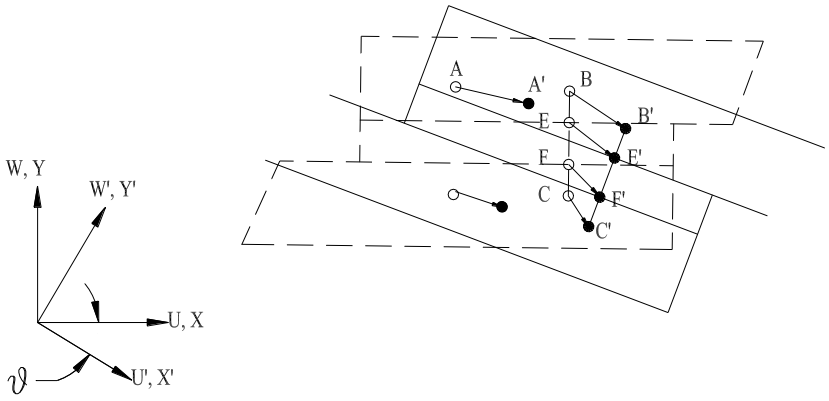

Figure 4.19. Translation and rotation of the specimen and final location of points.

Displacements in the direction of load are denoted by U, and displacements perpendicular to the direction of load are denoted by W. For example U_C is the displacement of point C with respect to original coordinate system (X-Y) in the direction of load (X-direction) and U'_C is in the rotated direction (X'-direction). Figure 4.19 shows the initial and final locations of the points of interest. It also shows X'-Y' as the rotated coordinate system and X-Y as the original coordinate system. Here, the angle of rotation, θ, from Figure 4.20, is calculated as

$$\tan\theta = \frac{W_B - W_A}{U_B - U_A + \frac{L}{2}} \tag{4.3}$$

Because θ and $(U_B - U_A)$ are very small, equation (4.3) reduces to

$$\theta = \frac{W_B - W_A}{\frac{L}{2}} \tag{4.4}$$

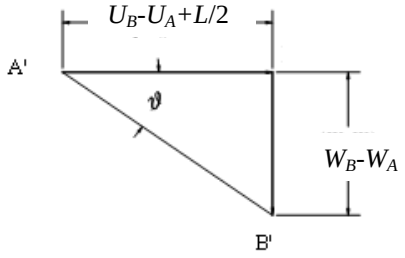

Figure 4.20. Angle of rotation of the specimen. A' and B' show the final locations of A, and B, respectively.

As the specimen rotates, the average shear strain of the adhesive, $\gamma_{average}$, is calculated as

$$\gamma_{average} = \frac{U'_E - U'_F}{t} \tag{4.5}$$

In equation (4.5), U'_E and U'_F are the displacement of points E and F in the X'-direction, the apparent shear strain is determined by

$$\gamma_{apparent} = \frac{(U'_B - U'_C) - (\frac{p-t}{p})(U'_{BM} - U'_{CM})}{t} \tag{4.6}$$

Here, U'_B and U'_C represent displacements of B and C in the X'-direction (Figure 4.19) of the adhesive specimen, while U'_{BM} and U'_{CM} represent displacement of B and C in the X'-direction of the all-titanium specimen with the same dimensions as the specimen with the bond present but with the adhesive replaced by titanium. In equation (4.6), (U'_B-

U'_C) includes both displacements of titanium (adherend) and adhesive. But based on the assumption that the displacement field between B and C is linear, the portion of displacement taken by the titanium must be subtracted from (U'_B-U'_C) to determine the $\gamma_{appaent}$. The portion of displacement taken by the titanium is (U'_{BM}-U'_{CM}) (p-t)/p).

4.2.2 Sources of Error

Basically, three sources of error can arise based on the test procedure and configuration:

1. The average shear strain differs with bondline thickness and the shear modulus of adhesives which is primarily due to the non-uniform shear strain and stress distribution with thickness and with the direction of load. This was one of the primary sources of errors [14,18].
2. Equation (4.6), which assumes linear displacement field, was not well represented for calculating the relative displacements of points from B to E, and F to C and for all-titanium specimen from B to C [14,18].
3. Errors, if any, can be caused by the rotation of the fixture and resulting readings from the laser extensometer.

4.2.3 Finite Element Analysis

Finite element analyses were conducted to simulate the mechanical behavior of ASTM D 5656 specimens. This was done for both normally bonded and all-titanium specimens under tensile loading. Before executing the finite element models of the ASTM D5656 specimen, a comparison of the 3D model, plane strain model, and plane stress model was performed on a 0.12 inch thick adhesive ASTM D 5656 specimen by applying a tensile load of 1,000 lbf. It was determined from Table 4.19 that the relative

displacement of B with respect to C was the same for the 3D model and plane strain models, i.e., 0.00214 inch, as shown in the relative displacement in Table 4.19. Based on the displacement of points A, B, C, E, and F, a comparison on different models was made which is shown in Figure 4.21. It can be concluded from Table 4.19 that the relative displacements of points, i.e., (U_B-U_C) and (U_E-U_F) which are the parameters of interest for calculating shear strain, the result from the plane strain finite element model, is the same as the original specimen analysis, which is the 3D model. Hence, all models were executed as plane strain analyses.

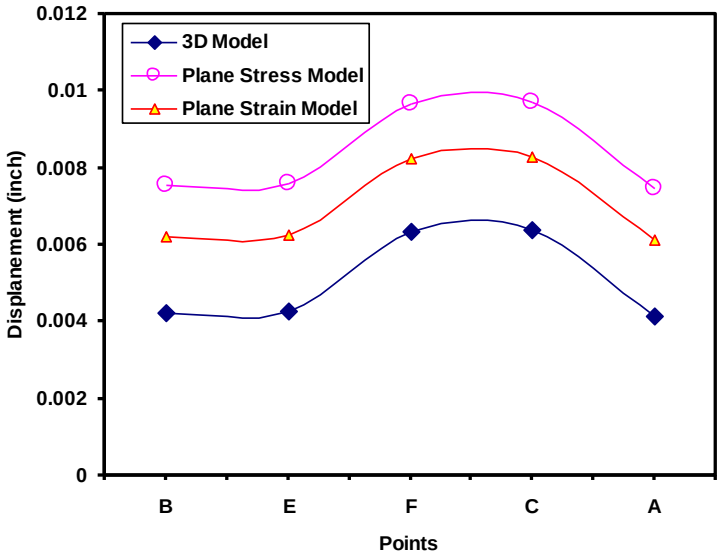

Figure 4.21. Comparison of plane stress and plane strain models with 3D models.

Correction factors for errors listed in Section 4.2.2 were determined for ASTM D 5656 specimens after executing finite element models of adhesive thicknesses 0.12 inch, 0.08 inch, 0.04 inch, 0.01 inch, and 0.001 inch with different shear moduli of adhesive (100 ksi, 150 ksi, 200 ksi and 250 ksi) and the all-titanium specimen. From the finite element models it was evident that the adherends in the overlap rotate due to the eccentric load transfer via the adhesive/adherend interfaces, as shown in Figure 4.22.

TABLE 4.19

DISPLACEMENTS OF A, B, C, D, E, AND F AND RELATIVE DISPLACEMENTS

ASTM D5656 model	Location	Displacement in X-Direction U (inches)	Relative of B wrt. C in X-Direction U_B-U_C (inches)	Relative of E wrt. C in X-Direction U_E-U_F (inches)
3D Model	B	6.38E-03	2.14E-03	2.10E-03
	E	6.36E-03		
	F	4.26E-03		
	C	4.24E-03		
	A	6.18E-03		
Plane Stress	B	9.70E-03	2.17E-03	2.14E-03
	E	9.68E-03		
	F	7.54E-03		
	C	7.53E-03		
	A	9.48E-03		
Plane Strain	B	8.36E-03	2.14E-03	2.10E-03
	E	8.24E-03		
	F	6.14E-03		
	C	6.22E-03		
	A	8.14E-03		

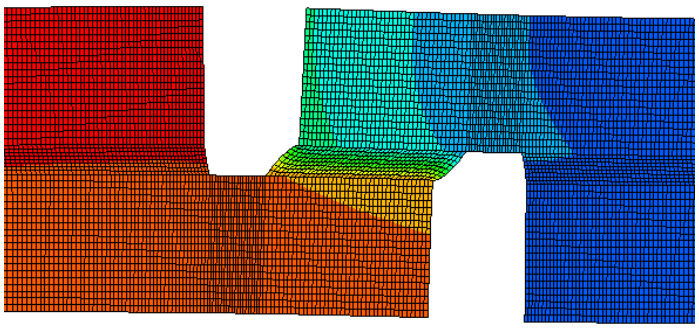

Figure 4.22. Rotation of overlap region of ASTM D 5656 FEM.

From the simulated models (finite element analysis), it was very evident that the maximum stresses and strains were maximum, adjacent to the overlap region. One other

major conclusion was regarding the non-uniform stress-strain distribution through the thickness of the adhesive [18]. In the ASTM D 5656 test procedure, the strain between points E and F was used to determine the shear modulus of adhesive. Hence accuracy was given much importance in determining the shear strain. Following description shows how the finite element models (ASTM D 5656 model) were effectively used in determining the shear strain and the associated results [18].

Assuming the joint undergoes shear and considering the coordinate transformation, as shown in Figure 4.19, the relative displacement between E and F for an ASTM D 5656 specimen with adhesive, (U'_E-U'_F), in the rotated direction is calculated as

$$U'_E - U'_F = (U_E - U_F)\cos\theta - (W_E - W_F + t)\sin\theta \tag{4.7}$$

where t is the distance between E and F, and t is the adhesive thickness. The average shear strain between points E and F, which is directly related to their relative displacements, is determined by equation (4.5). Replacing the $\gamma_{apparent}$ of equation (4.6) with $\gamma_{average}$ of equation (4.5) into equation (4.1), the adhesive shear modulus from ASTM test, G_{ASTM}, is then calculated as

$$G_{ASTM} = \frac{\tau_{average}}{\left(\frac{U'_E - U'_F}{t}\right)} \tag{4.8}$$

Figure 4.23 shows the calculated G_{ASTM} as a function of bondline thickness based on equation (4.8) with U'_E and U'_F determined from the finite element analysis. The horizontal line in Figure 4.23 represents the true shear modulus G_{true} of the adhesive. The adhesive shear modulus, G_{ASTM} and the input material property in the finite element model G_{true}, were compared for different adhesives with different adhesive thicknesses as

shown in Figure 4.23. It was well evident that the shear strain is non-uniform along the thickness. Shear modulus thus determined was a function of bondline thickness and real value of shear modulus. Thus the "recovered" shear modulus, G_{true}, of the adhesive was derived using non-linear regression analysis of the data points in Figure 4.23 [18].

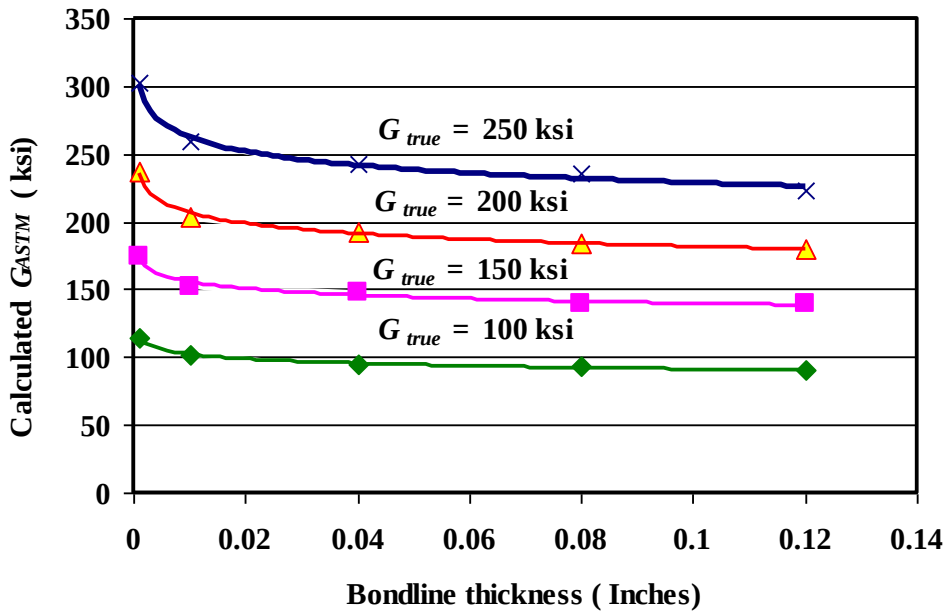

Figure 4.23. Calculated G_{ASTM} from finite element model.

A linear function between $G_{recovered}$ and the calculated G_{ASTM} is obtained in the form of

$$G_{recovered} = C_1 G_{ASTM} + C_2 \tag{4.9}$$

with

$$C_1 = 1.28t^{0.068} \tag{4.10}$$

$$C_2 = -0.07 + 10.58e^{-83.6t} \tag{4.11}$$

Variables C_1 and C_2 in equation (4.9) are functions of adhesive thickness, t, only and are independent of the shear modulus of adhesive. Variations of C_1 and C_2 with respect to adhesive thickness, t, are shown in Figures 4.24 and 4.25, respectively.

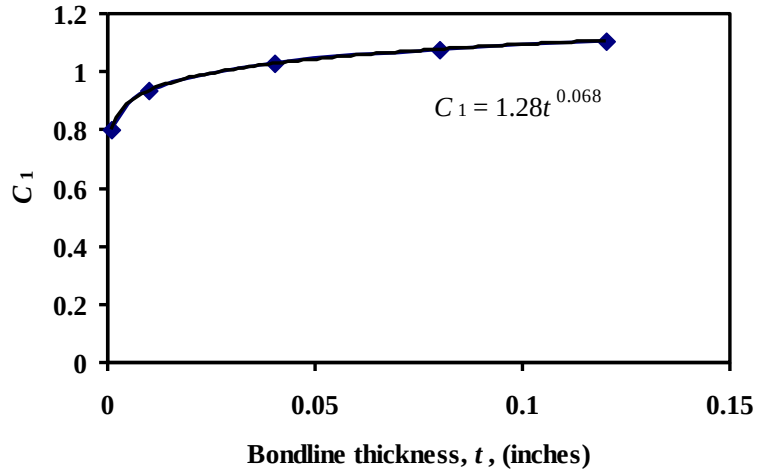

Figure 4.24. Variation of C_1 with respect to adhesive thickness.

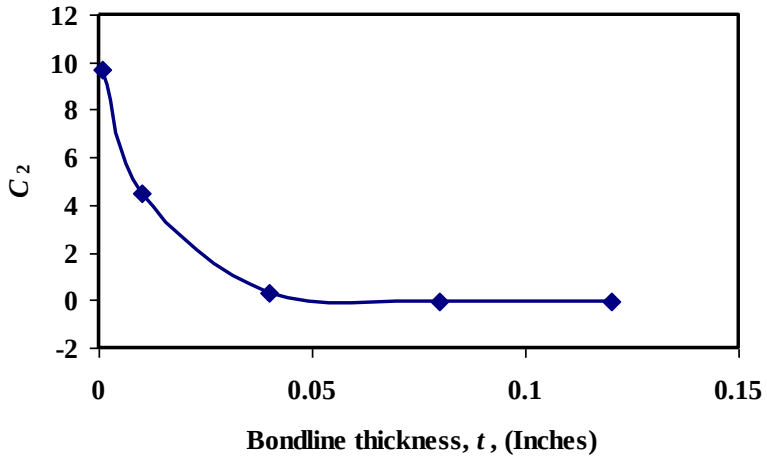

Figure 4.25 Variation of C_2 with adhesive thickness.

The important conclusion that was made after analyzing the models was that, when the bondline thickness was about 0.02 inch, the calculated value of G_{ASTM} was almost the same as the true shear modulus of adhesive. A comparison of G_{ASTM} and

$G_{recovered}$ is shown in Table 4.20. Based on the ASTM procedures, (U'_E-U'_F) is equal to (U'_B-U'_C)-(p-t)(U'_{BM}-U'_{CM})/p based on the assumption of a linear displacement field in the all-titanium sample from B to C.

TABLE 4.20

COMPARISON OF CALCULATED G_{ASTM} and $G_{recovered}$

	G_{true} =100 ksi		G_{true} =150 ksi		G_{true} =200 ksi		G_{true} =250 ksi	
t	G_{ASTM}	$G_{recovered}$	G_{ASTM}	$G_{recovered}$	G_{ASTM}	$G_{recovered}$	G_{ASTM}	$G_{recovered}$
0.12	90	100	135	153	179	199	224	248
0.08	193	100	140	150	185	199	235	254
0.04	95	98	148	152	192	198	242	249
0.01	101	99	153	147	203	197	259	247
0.001	115	102	175	150	237	199	302	251

As the displacements are recorded on points B and C, which also include shear strain in the titanium region, (U'_E-U'_F) in the adhesive region is calculated as

$$U'_E - U'_F \approx (U'_B - U'_C) - \left(\frac{p-t}{p}\right)(U'_{BM} - U'_{CM}) \tag{4.12}$$

Equation 4.12 is derived by assuming the condition that the shear strain distribution within the titanium-adhesive specimen and the all-titanium specimen is the same, and the shear strain distribution between points B and C for the all-titanium specimen in the X-direction is constant. Due to the non-constant shear strain distribution in the all-titanium specimen, a correction factor F_a is needed to convert (U'_{BM}-U'_{CM}) (p-t)/p to ($U'_B - U'_E$) + ($U'_F - U'_C$).

The correction factor F_a, for all-titanium specimen is determined from

$$(U'_B - U'_E) + (U'_F - U'_C) = F_a\left(\frac{p-t}{p}\right)(U'_{CM} - U'_{BM}) \tag{4.13}$$

Figure 4.26 shows F_a as a function of adhesive shear modulus, G_{true}, and bondline thickness, t. It can be seen that the change of F_a for varying adhesive shear moduli is almost negligible.

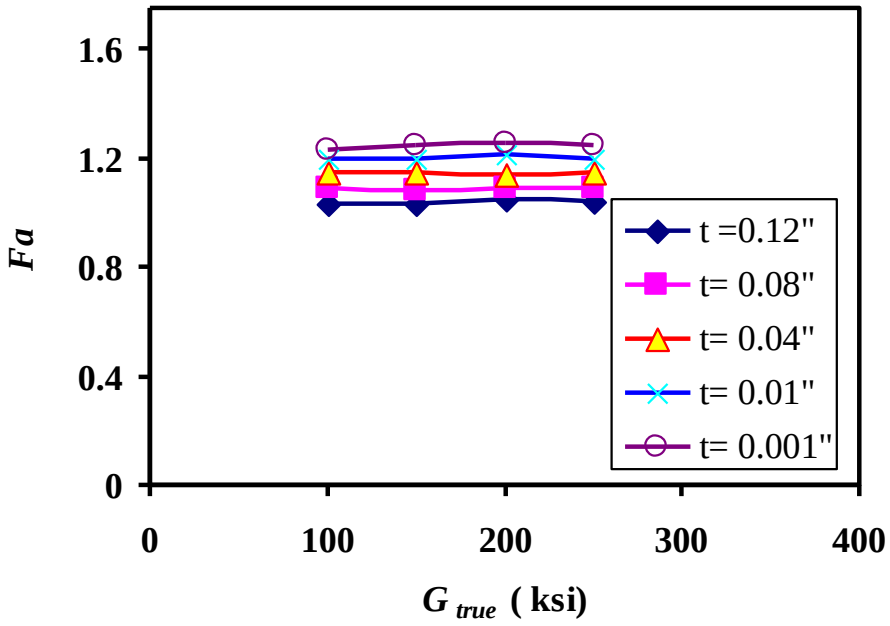

Figure 4.26. F_a as a function of t and G_{true}.

A linear regression yields F_a as a function of bond line thickness as

$$F_a = -1.751t + 1.23 \tag{4.14}$$

The variation of F_a with respect to t is given in Figure 4.27.

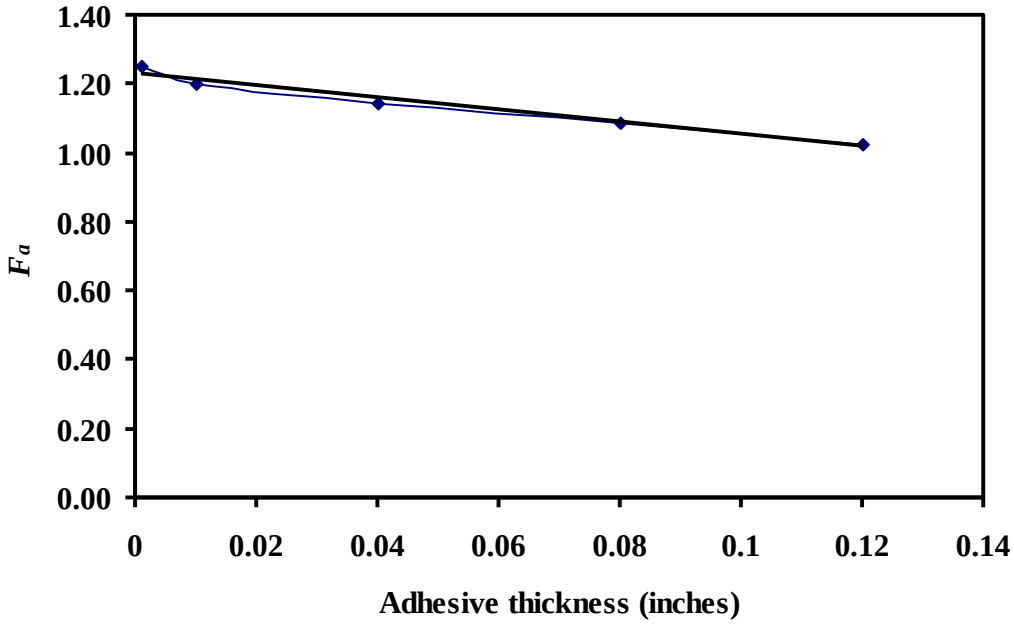

Figure 4.27. Variation of F_a with respect to *t*, adhesive thickness.

While using the laser extensometer and the designed fixture, since there are four pins on each side of the specimen and these fixtures pins are inserted into the holes drilled at A and B, and D and C, the readings recorded are the relative displacements of midpoint of A and B and the midpoint of D and C. The initial and final positions of the overlap region of the specimen are shown in Figure 4.28. The initial position of the specimen along with the fixture is shown by hidden lines, and the final position is shown by continuous lines. In Figure 4.28, the original coordinate system is represented by X-Y and the rotated coordinate system by X'-Y'. Due to the antisymmetric geometry of the specimen and loading, and from the finite element analyses, it was concluded that the relative displacement in the X'-direction of the midpoint of points A and B with respect to the midpoints of D and C is the same as the relative displacement of B with respect to C in the X'-direction, that is

$$U'_B - U'_C = \left(\frac{U'_A + U'_B}{2}\right) - \left(\frac{U'_C + U'_D}{2}\right) \tag{4.15}$$

Thus the displacements (U'_B-U'_C) and (U'_{BM}-U'_{CM}) can be measured from the readings of the laser extensometer.

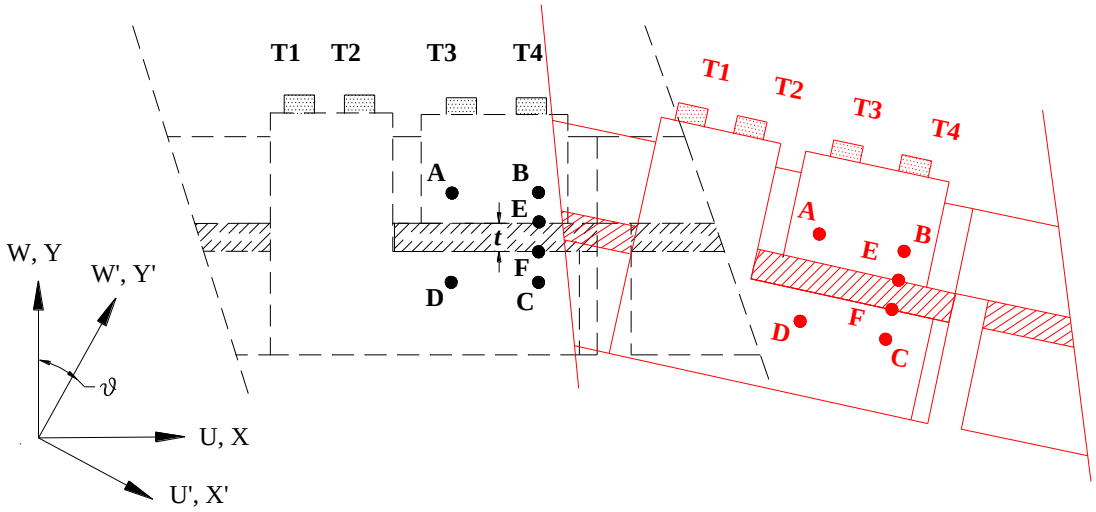

Figure 4.28. Initial and final positions of fixture and specimen.

While measuring the displacements of points B and C using the laser extensometer, the fixture rotates due to its variable arm length at an angle, θ, as shown in Figure 4.28. The relative displacements of B and C must be calculated in the rotated coordinate system, as shown in Figure 4.28. Therefore, the displacement vector in the X'-direction of point B with respect to C is calculated as

$$U'_B - U'_C = (U_B - U_C)\cos\theta - (W_B - W_C + p)\sin\theta \tag{4.16}$$

where p is the distance between B and C. The distance between B and the adhesive/adherend interface and the distance between C and the adhesive/adherend interface is 0.042 inch, so p is calculated as

$$p = 2(0.042) + t \tag{4.17}$$

Depending on the measurement mode selected, the laser extensometer successively measures the distance between the front edges of targets T1 and T2, T2 and T3, and T3 and T4 successively during each scan. As shown in Figure 4.28, T1 is the "leg" which is connected to the "L-shaped" fixture on the port side, T2 is connected to "L-shaped" fixture on the star side, T3 on the "square-shaped fixture" on the port side, and T4 on the "square-shaped fixture" on the star side. During testing, the specimen undergoes a translation as well as rotation, as shown in Fig 4.28. Since the beam is perpendicular to the X-direction, as shown in Figure 4.28, the laser reads the distance between targets (legs) in the original coordinate system.. The relative displacements of the two adherends on the port side are derived by considering the summation of distances between T2 and T1, and T3 and T2. On the star side, the relative displacements between the two adherends are derived by considering the summation of the distances between T3 and T2, and T4 and T3. The laser extensometer scans the distance between T2 and T1, T3 and T2 and T4 and T3. The equations for laser extensometer readings are determined as follows. From Figure 4.28, considering the initial position of the specimen (shown by hidden lines), the position vector of point C from the origin O represented by $\vec{C}$ is

$$\vec{C} = C_X \vec{i} + C_Y \vec{j} \tag{4.18}$$

where $\vec{i}$ and $\vec{j}$ are the unit vectors in the direction of the X and Y axes, respectively, as shown in Figure 4.28. Similarly, the position vector of point B from origin O represented by $\vec{B}$ is given by

$$\vec{B} = B_X \vec{i} + B_Y \vec{j} \tag{4.19}$$

The relation between position vector B and position vector C is

$$B_X \vec{i} + B_Y \vec{j} = C_X \vec{i} + C_Y \vec{j} + p\vec{j} \tag{4.20}$$

B_X and C_X are of the same magnitude, since point B is directly above point C. The location of targets T1 and T3 where the reflective tapes are attached on the port side is shown in Figure 4.29. T2 and T4 are on the star side, and their locations are shown in Figure 4.30. In Figure 4.29, $d_{Q/port/X,}$ and $d_{Q/port/Y}$ define the location of T1 from point C with respect to the initial coordinate system X-Y on the port side, $d_{P/port/X}$ and $d_{P/port/Y}$ are the locations of reflective tapes of the laser extensometer on T3 from point B on the port side, $d_{Q/star/X}$ and $d_{Q/star/Y}$ are the location of reflective tapes on T2 on the star side, and $d_{P/star/X}$ and $d_{P/star/Y}$ define the location of reflective tapes on T4. The initial location of reflective tapes on T1, T2, T3, and T4 is given by equations (4.21), (4.22), (4.23), and (4.24), respectively.

$$T1_{initial} = C_X \vec{i} + C_Y \vec{j} + (-d_{Q/port/X} \vec{i} + d_{Q/port/Y} \vec{j}) \tag{4.21}$$

$$T2_{initial} = C_X \vec{i} + C_Y \vec{j} + (-d_{Q/star/X} \vec{i} + d_{Q/star/Y} \vec{j}) \tag{4.22}$$

$$T3_{initial} = B_X \vec{i} + B_Y \vec{j} + (-d_{P/port/X} \vec{i} + d_{P/port/Y} \vec{j}) \tag{4.23}$$

$$T4_{initial} = B_X \vec{i} + B_Y \vec{j} + (-d_{P/star/X} \vec{i} + d_{P/star/Y} \vec{j}) \tag{4.24}$$

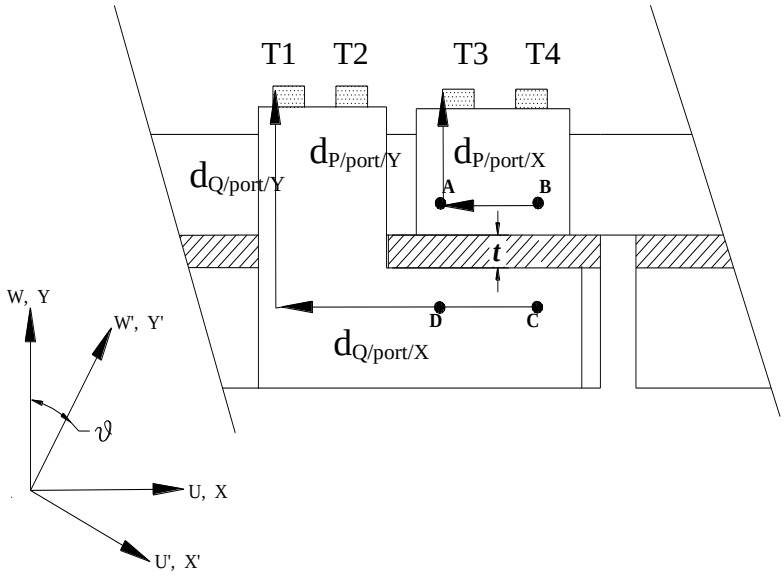

Figure 4.29. Locations of T1 and T3 on the port side of the specimen.

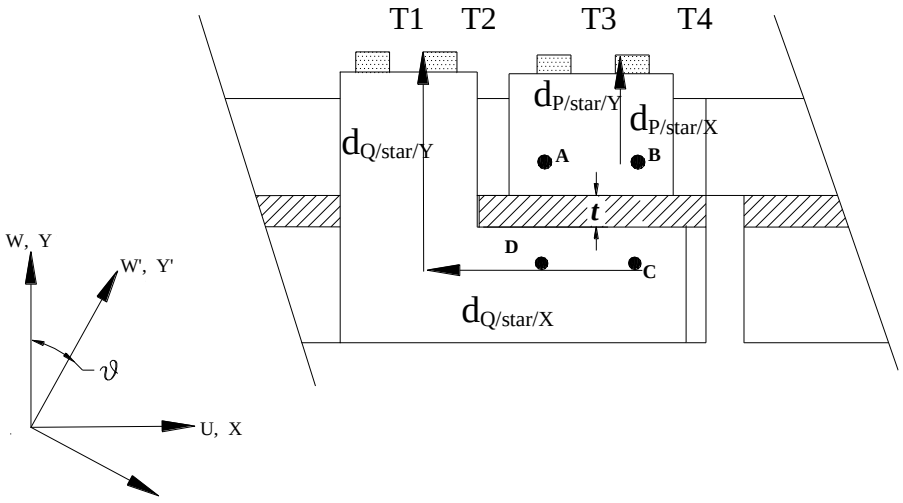

Figure 4.30. Locations of T2 and T4 on the star side of the specimen.

The initial distances between T1 and T2, T3 and T2, and T4 and T3 are represented by $T21_{initial}$, $T32_{initial}$, and $T43_{initial}$, respectively, and since the laser extensometer scans the distances parallel to the direction of load or in the X-direction only, the displacement vector component in the direction of X is considered. Hence, the components of $T21_{initial}$, $T32_{initial}$, and $T43_{initial}$ in the X-direction are given by $T21_{initial/X}$, $T32_{initial/X}$, and $T43_{initial/X}$, respectively, and are represented in equations (4.26), (4.27), and (4.28). For example, the initial distance between T1 and T2 is given by

$$T21_{initial} = (-d_{Q/star/X} + d_{Q/port/X})\vec{i} + (d_{Q/star/Y} - d_{Q/port/Y})\vec{j} \tag{4.25}$$

The component of $T21_{initial}$ in the X- direction, $T21_{initial/X}$, is given by

$$T21_{initial/X} = (-d_{Q/star/X} + d_{Q/port/X}) \tag{4.26}$$

Similarly, the components of $T32_{initial}$ and $T43_{initial}$ in the X-direction are given by

$$T32_{initial/X} = (B_X - C_X) + (-d_{P/port/X} + d_{Q/star/X}) \tag{4.27}$$

$$T43_{initial/X} = (-d_{P/star/X} + d_{P/port/X}) \tag{4.28}$$

The final location of T1 is calculated by considering both the translation of point C and the rotation of the fixture about point C, as shown in Figure 4.28, as

$$T1_{final} = U_C\vec{i} + W_C\vec{j} + \vec{C} + (-d_{Q/port//X}\cos\theta + d_{Q/port//Y}\sin\theta)\vec{i} + (d_{Q/port//X}\sin\theta + d_{Q/port//Y}\cos\theta)\vec{j} \tag{4.29}$$

where U_C and W_C are the displacement vectors of point C after the load is applied, and θ is the angle of rotation. Similarly, the final positions of T2, T3, and T4 are represented by equations (4.30), (4.31), and (4.32), respectively.

$$T2_{final} = U_C\vec{i} + W_C\vec{j} + \vec{C} + (-d_{Q/star/X}\cos\theta + d_{Q/star/Y}\sin\theta)\vec{i} + (d_{Q/star/X}\sin\theta + d_{Q/star/Y}\cos\theta)\vec{j} \tag{4.30}$$

$$T3_{final} = U_B\vec{i} + W_B\vec{j} + \vec{B} + (-d_{P/port//X}\cos\theta + d_{P/port//Y}\sin\theta)\vec{i} + (d_{P/port//X}\sin\theta + d_{P/port//Y}\cos\theta)\vec{j} \tag{4.31}$$

$$T4_{final} = U_B\vec{i} + W_B\vec{j} + \vec{B} + (-d_{P/star//X}\cos\theta + d_{P/star//Y}\sin\theta)\vec{i} + (d_{P/star//X}\sin\theta + d_{P/star//Y}\cos\theta)\vec{j} \tag{4.32}$$

where U_B and U_C are the displacements in the X-direction of location B, and C, respectively, while W_B and W_C are its displacements in the Y-direction. The components of final distance in the X-direction between T1 and T2, T3 and T2, and T4 and T3 are represented by $T21_{final/X}$, $T32_{final/X}$, and $T43_{final/X}$, respectively and are given in equations. (4.33), (4.34), and (4.35), respectively.

$$T21_{final//X} = (-d_{Q/star/X} + d_{Q/port/X})\cos\theta + (d_{Q/star/Y} - d_{Q/port/Y})\sin\theta \tag{4.33}$$

$$T32_{final//X} = (U_B - U_C) + (B_X - C_X) + (-d_{P/port/X} + d_{Q/star/X})\cos\theta + (d_{P/port/Y} - d_{Q/star/Y})\sin\theta \tag{4.34}$$

$$T43_{final//X} = (-d_{P/star/X} + d_{P/port/X})\cos\theta + (d_{P/star/Y} - d_{P/port//Y})\sin\theta \tag{4.35}$$

Laser extensometer measures the change in displacement of T1 and T2, T2 and T3, and T3 and T4 in the X-direction and are represented by $\Delta T21_X$, $\Delta T32_X$, and $\Delta T43_X$, respectively, where $\Delta T21_X$, $\Delta T32_X$, and $\Delta T43_X$ are calculated as

$$\Delta T21_X = (T21_{final/X} - T21_{initial/X}) \tag{4.36}$$

$$\Delta T32_X = (T32_{final/X} - T32_{initial/X}) \tag{4.37}$$

$$\Delta T43_X = (T43_{final/X} - T43_{initial/X}) \tag{4.38}$$

The sum of the distances calculated from $\Delta T21_X$ and $\Delta T32_X$ gives the reading corresponding to the relative displacement of B with respect to C in the X-direction on the port side. Similarly on the star side, the sum of $\Delta T32_X$ and $\Delta T43_X$ gives the measurement corresponding to relative displacement of B with respect to C on the star side. The calculated relative displacement of B with respect to C from the port side is represented by $\Delta T_{port/X}$ and on the star side is represented by $\Delta T_{star/X}$ and are determined as

$$\Delta T_{port/X} = \Delta T21_X + \Delta T32_X \tag{4.39}$$

$$\Delta T_{star/X} = \Delta T32_X + \Delta T43_X \tag{4.40}$$

Hence, the relative displacement of point B with respect to C on the port side from the readings corresponding to laser extensometer is

$$\Delta T_{port//X} = (U_B - U_C) + (d_{P/port/X} - d_{Q/port/X})(1-\cos\theta) + (d_{P/port/Y} - d_{Q/port/Y})(\sin\theta) \quad (4.41)$$

and the relative displacement of point B with respect to C on the star side from the readings corresponding to laser extensometer is

$$\Delta T_{star/X} = (U_B - U_C) + (d_{P/star/X} - d_{Q/star/X})(1-\cos\theta) + (d_{P/star/Y} - d_{Q/star/Y})(\sin\theta) \quad (4.42)$$

According to the design of the fixture, ($d_{P/star/X} - d_{Q/star/X}$) is the same as ($d_{P/port/X} - d_{Q/port/X}$), and ($d_{P/star/Y} - d_{Q/star/Y}$) is the same as ($d_{P/port/Y} - d_{Q/port/Y}$). Hence, the measurements from both port side and star side are the same.

The parameters $d_{Q/port/X}$, $d_{P/port/X}$, $d_{Q/port/Y}$, and $d_{P/port/Y}$ are based on fixture design (Appendix F). $d_{Q/port/X}$ and $d_{P/port/X}$ are determined from the fixture design and are 0.525 inch and 0.183 inch, respectively. The terms ($d_{P/port/Y} - d_{Q/port/Y}$) and ($d_{P/star/Y} - d_{Q/star/Y}$) are a function of adhesive thickness, *t*. But the fixture is designed in such a way that for a "zero" thickness adhesive specimen, T1 and T3 lie on the same horizontal plane and hence, ($d_{Q/port/Y} - d_{P/port/Y}$) is equal to 0.084 inch. For a specimen with certain adhesive thickness, *t*, ($d_{Q/port/Y} - d_{P/port/Y}$) is equal to *p*, which is same as (0.084+*t*). Thus the relative displacement of point B with respect to C, irrespective of the side of the specimen, represented by ΔT_X, is calculated as

$$\Delta T_X = (U_B - U_C) - 0.342(1-\cos\theta) - p(\sin\theta) \quad (4.43)$$

From Figure 4.31, it was found that the relative displacement of B with respect to C calculated from the readings of laser extensometer, ΔT_X, is almost equal to (U'_B-U'_C), determined from equation (4.16).

A linear regression analysis was performed on the data points in Figure 4.31 to obtain the relationship between (U'_B-U'_C) and the corresponding measurement calculated from laser extensometer readings, ΔT_X

$$(U'_B - U'_C) = F_1(\Delta T_X) + F_2 \tag{4.44}$$

where F_1 and F_2 are

$$F_1 = 1.000 \tag{4.45}$$

$$F_2 = 3\text{E-}5 \tag{4.46}$$

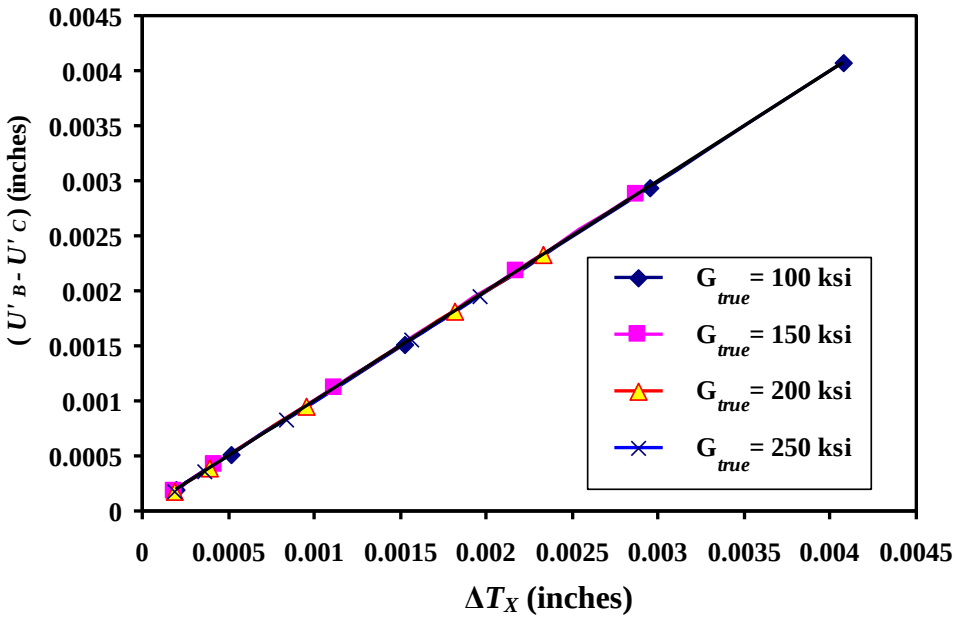

Figure 4.31. Relationship between relative displacement of B and C from laser extensometer readings (ΔT_X) and the real displacement of point B and C in the rotated direction.

Hence, inorder to convert the relative displacement of B with respect to C calculated from laser extensometer readings, ΔT_X, to (U'_B-U'_C), which is the original relative displacement of B with respect to C in the rotated coordinate system, correction factors F_1 and F_2 were included along with the calculated ΔT_X. Hence, the displacement of B

with respect to C in the rotated coordinate system can be determined from equation (4.44), where F_1 and F_2 are the correction factors. Similarly, for the all-titanium specimen, the same correction factors F_1 and F_2 are applicable to obtain the relative displacement of B with respect to C, (U'_{BM}-U'_{CM}). Hence, from the correction factors F_1 and F_2, it can be concluded that relative displacement of B with respect to C calculated from laser extensometer readings are almost the same as the real relative displacement of B with respect to C in the X'-direction.

Thus using ASTM D 5656 test data from the laser extensometer the average shear strain is determined by using

$$\gamma_{average} = \frac{(F_1 + F_2 \Delta T_X) - \{F_a (\frac{p-t}{p})(F_1 + F_2 (\Delta T_X)_M)\}}{t} \tag{4.50}$$

where $(\Delta T_X)_M$ is calculated from the laser extensometer readings of the all-titanium specimen, similar to that of ΔT_X. Thus, by substituting equation (4.50) for $\gamma_{apparent}$ in equation (4.5), the shear modulus of the adhesive can be determined. For adhesive thickness different from 0.02 inch, correction factors C_1 and C_2 are also included along with the determined shear modulus to determine the shear modulus value almost equal to that of G_{true} using equation (4.9). Figure 4.32 shows a flowchart for determining the shear modulus of an adhesive using ASTM D5656 with a laser extensometer.

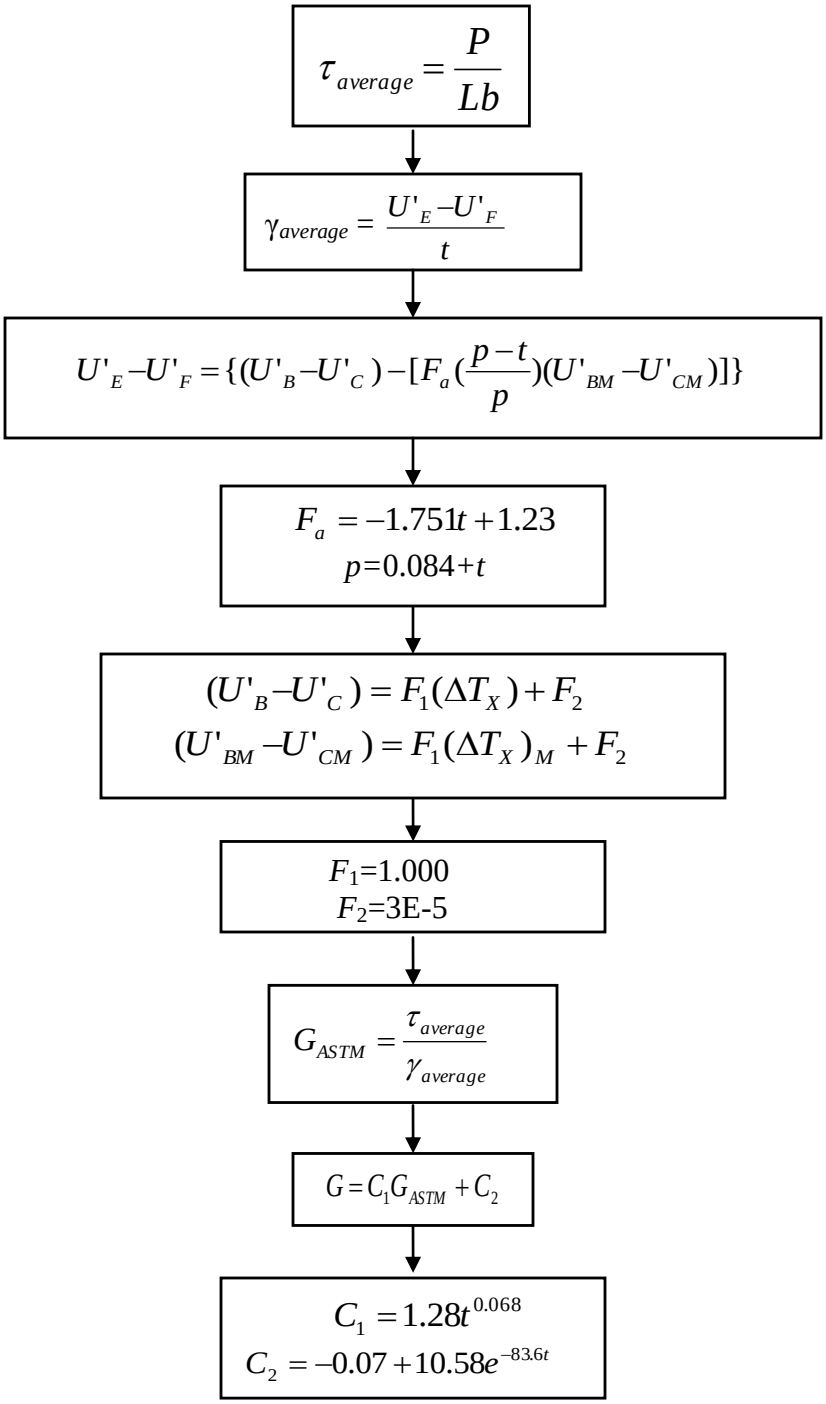

Figure 4.32. Flowchart to determine shear modulus of an adhesive for a given adhesive thickness ASTM D 5656 specimen using laser extensometer.

CHAPTER 5

CONCLUSIONS AND FUTURE WORK

Much advancement has been made in adhesives during the past years. From sheet metal applications to aerospace applications, advances in adhesive technology offer many advantages.

Tests were performed to determine the failure loads of certain adhesive single lap joints, both at room temperature and elevated temperature. As a result of this research, the methodology to obtain the shear modulus of adhesive from ASTM D 3165 (the test method that was generally used to obtain the shear strength of the adhesive joint specimen) was developed. In order to determine the adhesive shear modulus with a laser extensometer according to ASTM D 5656, test fixtures were designed to measure the displacements at respective locations on the specimen. The designed fixtures can be used to determine the stress-strain properties of adhesive at both room and elevated temperatures. Correction factors include while calculating the shear modulus of the adhesive, while using the laser extensometer and the designed fixture, were also determined.

It was found that, for different surface preparations of adhesive-A specimens, different failure loads were obtained. The shear modulus of the specimen that was determined using FEM was different for the same adhesive (adhesive-A) joint with different surface preparations. Hence, a greater number of specimens with adhesive-A must be tested. The method used on the ASTM D 3165 specimens in determining the shear modulus using FEM can also be used for ASTM D 1002 specimens. In order to prove that the correction factors determined for ASTM D 5656 specimens (using the laser

extensometer and the fixture) are accurate and sufficient, tests should be performed for known adhesive shear moduli.

REFERENCES

REFERENCES

[1] Patrick, R.C., *Treatise on Adhesion and Adhesive*, Marcel Dekker, New York, 1969, Vol. 2.

[2] Kutscha, D., "Mechanics of Adhesive-Bonded Lap-Type Joints: Survey and Review," Technical Report AFML-TDR-64-298, 1964.

[3] Kutscha, D., and Hofer, K.E., Jr., "Feasibility of Joining Advanced Composite Flight Vehicles," Technical Report AFML-TR-68-391, 1969.

[4] Edward, M. Petrie, *Handbook of Adhesives and Sealants*, McGraw-Hill Professional, New York, 1999, pp. 18-19.

[5] Kuno, J. K., "Structural Adhesives and Bonding," *Proceedings of the Structural Adhesives Bonding Conference*," El Segundo, CA., 1979.

[6] "Standard Test Method for Strength of Single-Lap-Joint Adhesively Bonded Metal Specimens by Tension Loading," *Annual Book of ASTM Standards*, Vol. 15.06, 1997, pp. 45-48.

[7] Volkersen, O., *Luftfarhtforschung* 15, 1938, pp. 41-47.

[8] Goland,M. and Reissner, E., "The Stress in Cemented Joints," *Journal of Applied Mechanics*, March 1944, pp. A17-A27.

[9] Hart-Smith, L. J., "Adhesive-Bonded Single Lap Joints," Douglas Aircraft Company., NASA Langley Report CR 112236, 1973.

[10] Hart-Smith, L. J., "Analysis and Design of Advanced Composite Bonded Joints," Douglas Aircraft Company., NASA Langley Report CR-2218, 1974.

[11] "Standard Test Method for Strength Properties of Adhesives in Shear by Tension Loading of Single Lap-Joint Laminated Assemblies" *Annual Book of ASTM Standards* 1997, Vol. 15.06, pp. 199-202.

[12] "Standard Test Method for Thick Adherend Metal Lap-shear Joints for Determination of the Stress-Strain Behavior of Adhesives in Shear by Tension Loading" *Annual Book of ASTM Standards* 1997, Vol. 15.06, pp. 470-475.

[13] Harter, P., "Investigation of Adhesive Test Methods for Thick Bondline Joints," Masters Degree Thesis, Department of Aerospace Engineering, Wichita State University, Wichita, Kansas, 2000.

REFERENCES (continued)

[14] Tomblin, J., Yang, C., and Harter, P., "Investigation of Thick Bondline Adhesive Joints," DOT/FAA/AR-01/33, FAA, William J. Hughes Technical Center, Atlantic City International Airport, NJ, June 2001.

[15] Tomblin, J., Harter, P., Seneviratne W., and Yang, C., "Characterization of Bond-line Thickness Effects in Adhesive Joints," *ASTM Journal of Testing and Evaluation*, Journal of Composites Technology and Research, Vol. 24, No. 2, April 2002, pp. 332-344.

[16] Tomblin, J., Seneviratne W., Escobar, P., and Yoon-Khian, Y., "Shear-Stress Data for Structural Adhesives," DOT/FAA/AR-02/97, FAA, William J.Hughes Technical Center, Atlantic City International Airport, NJ, Nov. 2002.

[17] Yang, C., Huang, H., Tomblin, J. S., and Oplinger, D. W., " Evaluation and Adjustments for ASTM D 5656 Standard Test Method for Thick-Adherend Metal Lap-Shear Joints for Determination of the Stress-Strain Behavior of Adhesives in Shear by Tension loading," *Journal of Testing and Evaluation*, Vol..1, Jan 2001, pp. 36-43.

[18] Yang, C. and Tomblin, J, Y., "Investigation of Adhesive Behavior in Aircraft Applications," DOT/FAA/AR-01/57, The FAA William J. Hughes Technical Center Technical Monitor was Peter Shyprykevich., Sept. 2001.

[19] Yang, C. and Tomblin, J, Y., "Analytical Modeling of ASTM Lap Shear Adhesive Specimens," DOT/FAA/AR-02/130, The FAA William J. Hughes Technical COTR was Peter Shyprykevich., Feb. 2003.

APPENDICES

APPENDIX A

AEROSHELL

The function of aeroshell is that it acts as a protective covering on a space craft during planetry missions. When the spacecraft enters a planetry atmosphere it produces immense heat on the spacecraft. The main purpose of aeroshell is to protect the "entry vehicle" (lander and rover) from this heat.

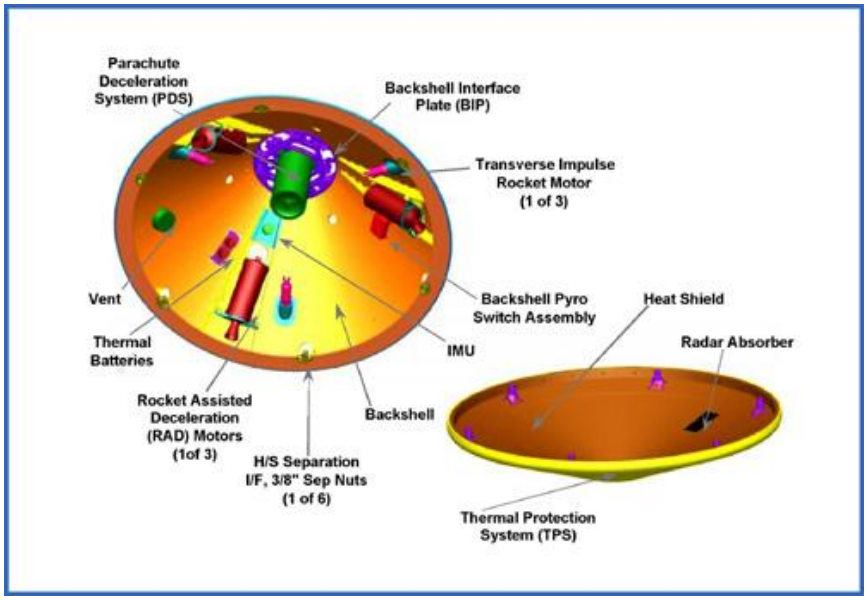

Figure A.1. Aeroshell [NASA].

Parts of Aeroshell

Two major components of aeroshell are:

- Heat shield
- Backshell

A space vehicle is prone to intense heating while it enters into the planetary atmosphere. The heat shield, which is the primary component protects the lander and

rover during this intense heat. One of the other major advantages of the heat shield is that it aerodynamically acts as the first "brake" for the spacecraft.

The backshell includes the following components

- A parachute
- The backshell electronics and batteries, separation nuts, rockets, and the parachute related equipments.
- A Litton LN-200 Inertial Measurement Unit (IMU). The function and purpose of this unit is to monitor and report the orientation of the backshell.
- Three large solid rocket motors which provide immense thrust
- Trasverese Impulse Rocket System: This includes three small rockets. The three rockets provide a horizontal force to the backshell. This extra force helps the backshell to orient vertically.

The major components of aeroshell is an honeycomb structure with graphite-epoxy face sheets. The outer portion of the aeroshell is a layer of phenolic honeycomb made from benzene. This phenolic honeycomb is filled with "ablator". The intense heat generated by atmospheric friction is dissipated by this ablator. It was invented for Mars lander missions. The ablator was designed and made to react chemically with the Martian atmosphere during entry and essentially dissipate heat away, and thereby slowing it down much faster which produces 10 "earth gees" of acceleration.

APPENDIX A (continued)

The backshell and heat shield are made of the similar materials as that of aeroshell. The heat shield has a thicker layer of the ablator, which are a unique blend of cork wood, binder and many tiny silica glass spheres. The backshell is covered with a very thin aluminized mylar blanket. This protects the whole unit from the cold of deep space.

APPENDIX B

ADHESIVES

Adhesive A

Adhesive A is a modified bisaleimide film adhesive with superior strength to 550ºF. It is moisture resistant and processes like conventional high-temperature epoxies.

Adhesive A requires refrigerated storage at 0ºF or below for maximum storage life. It may be cured for one hour at 350ºF plus a post cure of two hours at 475 ºF. The Heat-up rate to cure temperature is not critical, but should be between 2ºF and 7ºF per minute. Pressure should be applied before heating the parts to be bonded and maintained until the assembly gets is cooled down. No bonding pressure is required during the post cure. A step cure of 60 to 90 minutes at 250ºF under low pressure of 5-1 psi followed by one hour at 350ºF with full pressure will reduce adhesive flow during cure.

Adhesive H

Adhesive H is a condensation polymide adhesive supplied as a supported film with a woven fiberglass carrier. It is suitable for bonding metallic and non-metallic substrates as well as honeycomb structures. Adhesive H film adhesive can be processed at 350ºF, with a freestanding post cure at 550ºF. This adhesive film provides a service temperature of -67ºF to 550ºF and can be used for repair and radar transparent applications.

Adhesive C

Adhesive C is a flowable, one component, addition cure, self-bonding silicate rubber. It is readily cured at elevated temperatures to a tough silicone rubber, which bonds well to many substrates. Adhesive C is cured readily at temperatures ranging from

212ºF to 392ºF. Because of its relatively low viscosity and self bonding properties, it can also be employed as a flow-in gasket.

Adhesive D

Adhesive D is phenolic epoxy, capable of withstanding short-term exposure to 1,000ºF. It has the minimum recommended cure temperature of 350ºF and service temperature of 500ºF.

APPENDIX C

MODELS LE-01 LASER EXTENSOMETER

Model LE-01 extensometers (by Electronic Instrument research) are high-precision non-contacting units. Laser extensometers are used for strain measurement in materials testing. They employ a high-speed laser scanner to measure the spacing between reflective tape strips which are glued on a test specimen. The measurement range is from 0.3 to 3.2 inches (8 to 81 mm) on the LE-01 and the gage length is determined by the person performing the test. Smaller strains are accurately measured. This extensometer uses the state-of-the-art laser diode technology.

The scanning beam is always close to perpendicular to the specimen. The equipment minimizes sensitivity to distance between the extensometer and the test specimen. As the whole measurement is based on the reflected beam from the sample, no receiver is required behind the sample. The visible laser light is aimed at the specimen with a small inclination. The test specimen has small reflective tape strips set at the desired gage length. The extensometer displays the actual measured gage length. If desired, the zero buttons will offset the output to zero, so that the resultant reading during the test is just the resulting elongation due to the load applied. The analog output and RS-232 interface can be easily connected to the data acquisition systems. High temperature clip-on reflectors may be used as an alternate to tape reflectors for high temperature testing.

APPENDIX C (continued)

These high temperature reflective tapes can be used at temperatures up to 300ºF (150ºC). These are re-useable and available as an option. They are rated for use to 800ºF (425ºC).

Features

- Non-contacting design
- Ideal use in chambers
- Resolution of 1 micron, which is considered really high.
- Allows high elongation measurements (e.g.200% on a one inch gage length).

APPENDIX D

ATS 304 6/92 SERIES 3160 SPLIT BOX FURNACES

For basic laboratory and testing applications, ATS series 3160 split box furnaces are the ideal choice. Used in testing installations around the world, these furnaces are unmatched in quality. ATS series 3160 furnaces are available in a number of standard sizes, or they can be built specifications. A variety of options and accessories can be utilized to suit all the testing needs, including load train ports, thermocouples, viewports, gas ports, offsets or removable hinges, custom heating elements, muffles, liners, and more. The maximum temperature range of the split box furnace is 2,200ºF.

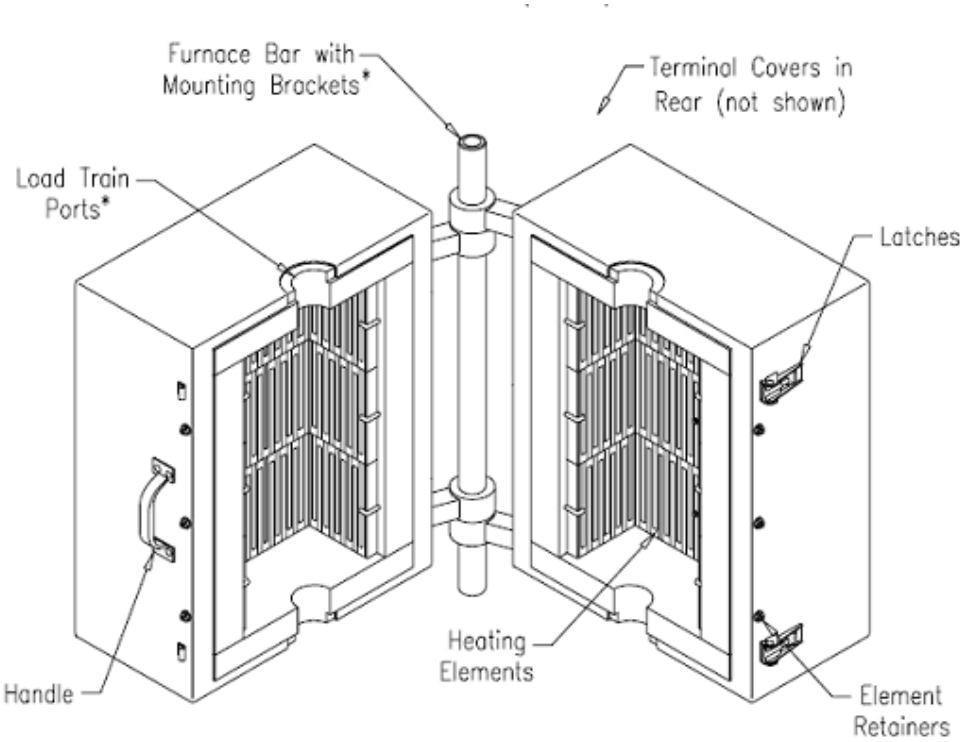

Figure D.1. ATS series 3160 split box furnace.

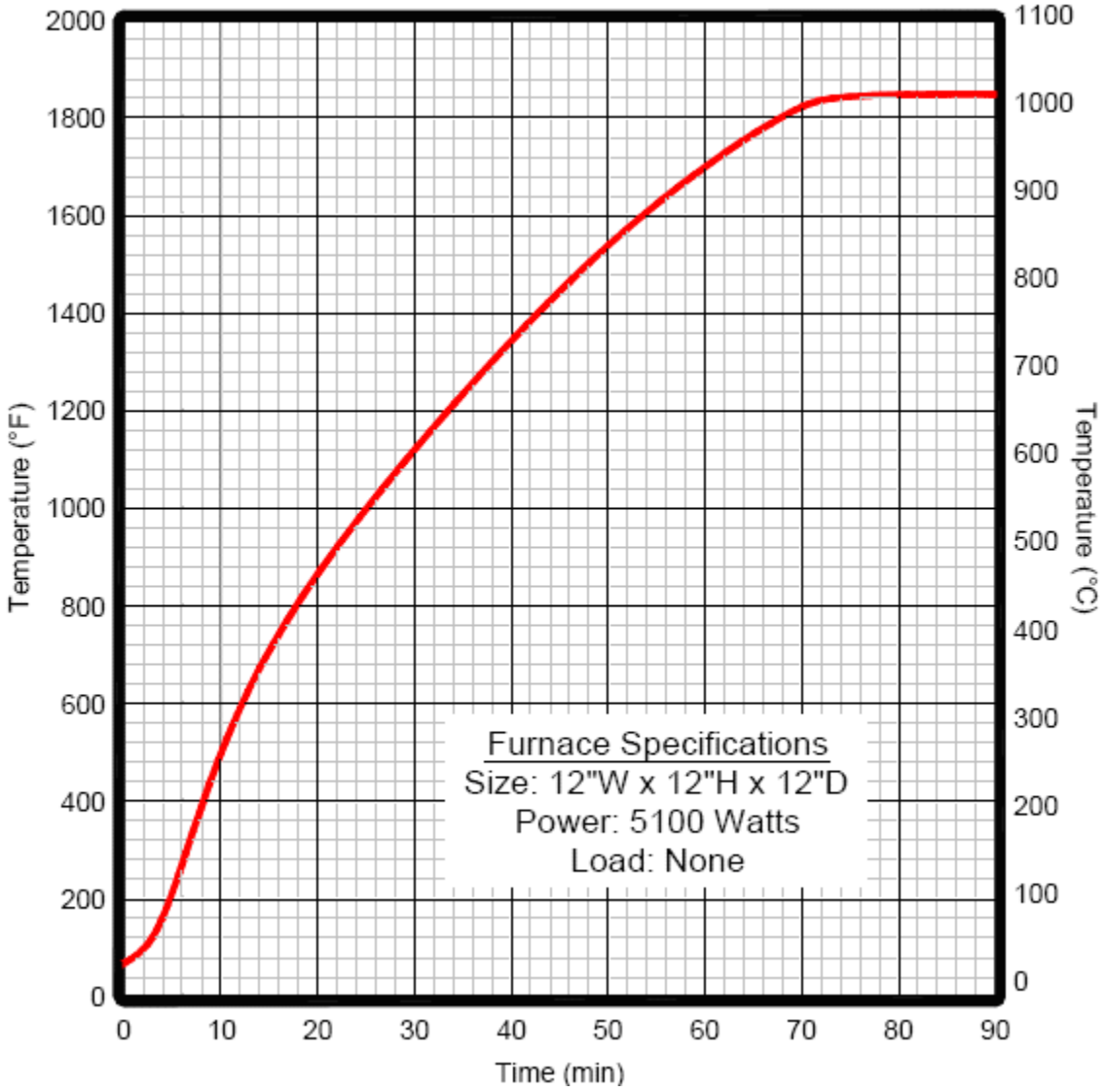

Figure D.2. Heat-up curve for ATS series 3160 split box furnace.

APPENDIX E

MTS 653 FURNACE

The family of MTS 653 furnaces is designed to use for a wide range of temperatures testing. These types of chambers are used for materials ranging from metals to composites to ceramics. This chamber is ideal for tension, compression, bend, and cyclic fatigue testing. Their center split design allows for simple access to specimen and fixture, which is very much helpful during testing. It is conveniently designed to separate the two halves. Exclusively designed mounting brackets are available for a variety of MTS and non-MTS load frames. One of the major parts of the furnace is the type R thermocouple and mounting bracket. The multi-zone option helps the thermocouples and temperature control for each zone inside the furnace. MTS high-temperature mechanical extensometers can also be used inside this furnace.

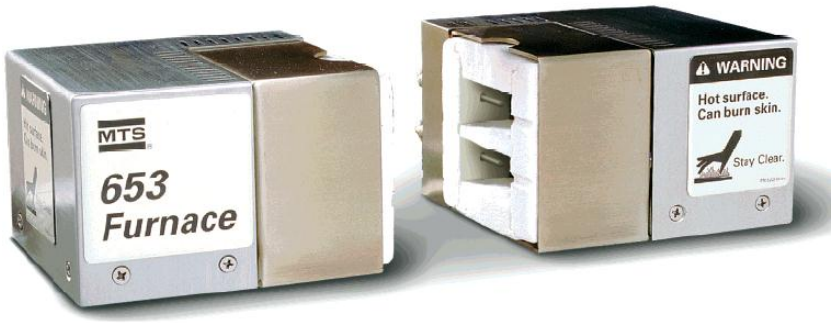

Figure E.1. MTS 653 furnace.

Features

- low heat loss and long life.

- multiple heating of zones.
- Good specimen and fixture access.
- PID control.
- Digital interfaces are available.
- SCR power relays embedded.

APPENDIX F

FIXTURE PARTS